Monthly Notices
of the
ROYAL ASTRONOMICAL SOCIETY
MNRAS **457,** 2173–2191 (2016) doi:10.1093/mnras/stw049

A lucky imaging multiplicity study of exoplanet host stars – II

C. Ginski,[1,2★] M. Mugrauer,[2] M. Seeliger,[2] S. Buder,[2,3] R. Errmann,[2,4] H. Avenhaus,[5] D. Mouillet,[6,7] A.-L. Maire[8] and S. Raetz[9]

[1]*Leiden Observatory, Leiden University, PO Box 9513, NL-2300 RA Leiden, the Netherlands*
[2]*Astrophysikalisches Institut und Universitäts-Sternwarte Jena, Schillergässchen 2, D-07745 Jena, Germany*
[3]*Max-Planck-Institut für Astronomie, Königstuhl 17, D-69117 Heidelberg, Germany*
[4]*Isaac Newton Group of Telescopes, Santa Cruz de La Palma, E-38700, Spain*
[5]*Departamento de Astronomìa, Universidad de Chile, Casilla 36-D, Santiago, Chile*
[6]*Université Grenoble Alpes, IPAG, F-38000 Grenoble, France*
[7]*CNRS, IPAG, F-38000 Grenoble, France*
[8]*INAF - Osservatorio Astronomico di Padova, Vicolo dell'Osservatorio 5, I-35122 Padova, Italy*
[9]*Scientific Support Office, Directorate of Science and Robotic Exploration, European Space Research and Technology Centre (ESA/ESTEC), Keplerlaan 1, NL-2201 AZ Noordwijk, the Netherlands*

Accepted 2016 January 6. Received 2015 December 4; in original form 2015 September 4

ABSTRACT

The vast majority of extrasolar planets are detected by indirect detection methods such as transit monitoring and radial velocity measurements. While these methods are very successful in detecting short-periodic planets, they are mostly blind to wide sub-stellar or even stellar companions on long orbits. In our study, we present high-resolution imaging observations of 60 exoplanet hosts carried out with the lucky imaging instrument AstraLux at the Calar Alto 2.2 m telescope as well as with the new Spectro-Polarimetric High-contrast Exoplanet REsearch (SPHERE) high-resolution adaptive optics imager at the ESO/VLT in the case of a known companion of specific interest. Our goal is to study the influence of stellar multiplicity on the planet formation process. We detected and confirmed four previously unknown stellar companions to the exoplanet hosts HD 197037, HD 217786, Kepler-21 and Kepler-68. In addition, we detected 11 new low-mass stellar companion candidates which must still be confirmed as bound companions. We also provide new astrometric and photometric data points for the recently discovered very close binary systems WASP-76 and HD 2638. Furthermore, we show for the first time that the previously detected stellar companion to the HD 185269 system is a very low mass binary. Finally, we provide precise constraints on additional companions for all observed stars in our sample.

Key words: astrometry – techniques: high angular resolution – planets and satellites: formation – binaries: visual – stars: individual: HD 185269 – stars: individual: Kepler-21.

1 INTRODUCTION

We live in a golden age for extrasolar planet discoveries. In the past decade several large radial velocity and transit surveys have discovered more than 1200 systems containing extrasolar planets (exoplanet.eu, as of 2015 July). While these indirect detection methods have been incredibly successful, they have a few inherent biases. In particular, while they are very sensitive to short-period companions (often in the order of days or weeks), they are blind to wide (sub-) stellar companions at several tens or hundreds of au. However, more than 50 per cent of all main-sequence stars in the Galaxy and approximately half of all solar-type stars are actually members of stellar multiple systems (Mathieu et al. 2000; Raghavan et al. 2010). It is thus of great interest to investigate the influence of stellar multiplicity on extrasolar planet formation and orbital evolution.

There have been a large number of theoretical and observational studies that investigated the influence of close and wide stellar companions on the various stages of the planet formation process. It is, for instance, believed that close stellar companions will truncate protoplanetary discs and shorten their dissipation time-scale. This has been observationally confirmed e.g. by Bouwman et al. (2006), who found a significantly reduced number of discs in binary systems in their *Spitzer* survey of the young η Cha star cluster. Other studies such as Kraus et al. (2012) find that this effect is dependent on the binary separation with significant drops of disc occurrences only observed for systems with separations smaller than ∼40 au.

In addition to the initial conditions and time-scales in the protoplanetary disc, stellar companions might also influence the accretion of planetesimals by exciting higher eccentricities and velocities

★E-mail: ginski@strw.leidenuniv.nl

which might lead to more destructive collisions (see e.g. Kley & Nelson 2007 or Paardekooper, Thébault & Mellema 2008). However, recent studies find that this effect might be mitigated by the gravitational force of sufficiently massive discs (Rafikov 2013).

Finally, stellar companions might have a major influence on the observed semimajor axis, inclination and eccentricity distributions of extrasolar planets. Studies by Fabrycky & Tremaine (2007) and Petrovich (2015) suggest that Kozai–Lidov-type interactions between planets and stellar companions, in combination with tidal friction, might explain some of the observed extreme short period orbits. Other studies (e.g. Naoz et al. 2011) suggest that such interactions could explain very eccentric planet orbits or spin-orbit misalignment. For a comprehensive overview of all these effects we suggest the article by Thebault & Haghighipour (2014).

To study these effects, it is necessary to find the true fraction of multiple stellar systems amongst extrasolar planet host stars. Diffraction- or seeing-limited imaging is a primary tool for this purpose, in particular to find multiple stellar systems with planets in S-type orbits, i.e. the planets orbit one of the stellar components of the system. This orbit configuration accounts for the majority of multiple stellar exoplanet systems (see e.g. Roell et al. 2012).

There have been a number of imaging studies in the past such as Eggenberger et al. (2007), Mugrauer, Neuhäuser & Mazeh (2007), Daemgen et al. (2009), Chauvin et al. (2011), Lillo-Box, Barrado & Bouy (2012), or more recently Dressing et al. (2014), Mugrauer, Ginski & Seeliger (2014), Mugrauer & Ginski (2015) and Wöllert et al. (2015).

In this work, we present the results of our ongoing multiplicity study employing the lucky imaging instrument AstraLux (Hormuth et al. 2008) at the Calar Alto 2.2 m telescope. In particular, we present results for 60 systems obtained between 2011 and 2015. Results prior to that can be found in the first publication of our survey in Ginski et al. (2012). Our targets are stars around which an exoplanet has been detected by radial velocity or transit observations and which have not yet been observed with high-resolution imaging. We further limit our sample to stars within ∼200 pc (with few exceptions) so that we are able to confirm detected companion candidates via common proper motion analysis. In addition to our lucky imaging observations, we complement our study with extreme adaptive optics supported images from the new planet hunting instrument Spectro-Polarimetric High-contrast Exoplanet REsearch (SPHERE) (Beuzit et al. 2008) at the ESO/VLT.

We derive astrometric and photometric data of all detected companion candidates and perform common proper motion analysis for all systems with more than one observation epoch. Finally, we provide detailed detection limits on all observed systems.

2 OBSERVATIONS AND DATA REDUCTION

The observations presented in this study were undertaken between 2011 July and 2015 March with the lucky imaging instrument AstraLux at the Calar Alto Observatory. In addition, we present data for one system which was taken with the new SPHERE planet hunting instrument at the ESO VLT during guaranteed time observations (GTO) in 2015 May.

For our lucky imaging observations, we used short exposures times in the same order as the coherence time of the atmosphere (e.g. Hormuth et al. (2008) measure a speckle coherence times at the Calar Alto of 36 ms). We then recorded a large number of individual images (typically 50 000) of which we only used subsets with the highest Strehl ratio (Strehl 1902) for final combination. The lucky imaging technique is described in detail in e.g. Law, Mackay & Baldwin (2006). All lucky imaging observations were undertaken using the SDSS *i* filter. The electron multiplying gain of the instrument was adjusted individually for each target to enable high signal to noise without saturating the primary star. We also adjusted the focus of the instrument several times during the night to ensure highest image quality. In our 2011, 2013 and 2014 observations in visitor mode, we used the full field of view of the detector of 24 × 24 arcsec with the shortest possible exposure time of 29.54 ms in frame transfer mode. For the brightest targets, we used shorter integrations times without frame transfer mode and less overall frames due to larger overheads, i.e. significantly increased readout time. In the 2015 observations in service mode the instrument was used in windowed mode, reading only half of the field of view. This enabled shorter exposure times of typically 15.03 ms. Details for each system are given in Table 1.

Data reduction of the lucky imaging data included flat-fielding with sky flats taken during dawn, as well as bias subtraction. Bias frames were taken before each science exposure with the same gain settings as the science target. After flat-fielding and bias subtraction, the Strehl ratio in each image was measured and then only the images with the 10, 5 and 1 per cent best Strehl ratios were aligned and combined, respectively.[1] For the final data reduction, we utilized the native AstraLux pipeline available at Calar Alto (described in detail by Hormuth et al. 2008), as well as our own pipeline for the reduction of lucky imaging data. Our own pipeline was used in all those (few) cases where the Calar Alto pipeline produced no output due to software malfunction. Final images with detected known companions as well as new companion candidates are shown in Figs 1 and 2. We show the 2013 data when available, since it is in general of slightly higher quality than the 2014 data due to better weather conditions (higher coherence time, no clouds). To enhance the contrast between the bright primary stars and the faint companion candidates, we have employed high pass filtering on the images.

In addition, we did use SPHERE's near-infrared camera IRDIS (Dohlen et al. 2008) in dual band imaging mode (Vigan et al. 2010) to image the HD 185269 system in *Y*, *J* and *H* band with broadband filters on 2015-05-02. The specific interest in this system was triggered by an observed elongation of the companion's point spread function (PSF) in our AstraLux observations. We used the minimal exposure time of 0.84 s without coronagraph and with neutral density filter, which led to only minor saturation of the core of the primary star's PSF in *Y* and *H* band, and no saturation in *J* band. For each filter setting, we took a total of 20 individual exposures for a total integration time of 16.8 s. All individual images in each band were median combined and then flat-fielded and dark subtracted. Since we did not apply a dither pattern in this very short observation sequence, we then used a bad pixel mask (created from flat and dark frames) to eliminate bad pixels. Finally, we combined both images of the dual imaging mode in each band. A resulting combined colour image is shown in Fig. 3.

3 ASTROMETRIC CALIBRATION AND MEASUREMENTS

The most reliable method to determine if individual companion candidates are bound to the systems around which they are discovered is to ascertain if they exhibit the same proper motion as the

[1] If not otherwise stated, we generally used the best 10 per cent images for subsequent analysis.

Table 1. Observation summary of all targets observed with AstraLux at the Calar Alto 2.2 m telescope. We give the total integration time for each target for a frame selection rate of 10 per cent.

Star	RA	Dec	Epoch	# of frames	Exposure time (ms)	Tot. integ. time (s)	Field of view (arcsec)
HD 2638	00 29 59.872 74	−05 45 50.4009	19-08-2014	50 000	29.54	147.70	24 × 24
HD 2952	00 33 10.394 67	+54 53 41.9440	19-08-2014	50 000	29.54	147.70	24 × 24
HD 5608	00 58 14.218 93	+33 57 03.1843	17-01-2013	50 000	29.54	147.70	24 × 24
HD 5891	01 00 33.192 04	+20 17 32.9381	17-01-2013	50 000	29.54	147.70	24 × 24
HD 8574	01 25 12.515 65	+28 34 00.1010	30-06-2013	50 000	29.54	147.70	24 × 24
HD 10697	01 44 55.824 84	+20 04 59.3381	20-08-2014	50 000	29.54	147.70	24 × 24
WASP-76	01 46 31.8590	+02 42 02.065	19-08-2014	50 000	29.54	147.70	24 × 24
HAT-P-32	02 04 10.278	+46 41 16.21	19-08-2014	60 000	29.54	177.24	24 × 24
HD 12661	02 04 34.288 34	+25 24 51.5031	20-08-2014	50 000	29.54	147.70	24 × 24
HD 13189	02 09 40.172 60	+32 18 59.1649	20-08-2014	50 000	29.54	147.70	24 × 24
HD 13908	02 18 14.560 56	+65 35 39.6988	19-08-2014	50 000	29.54	147.70	24 × 24
HD 15779	02 32 09.422 00	−01 02 05.6236	17-01-2013	50 000	29.54	147.70	24 × 24
HD 285507	04 07 01.226 53	+15 20 06.0989	20-08-2014	50 000	29.54	147.70	24 × 24
HD 290327	05 23 21.564 90	−02 16 39.4302	10-03-2015	50 000	15.03	75.15	12 × 12
HD 40979	06 04 29.942 14	+44 15 37.5940	10-03-2015	50 000	29.54	147.70	12 × 12
HD 43691	06 19 34.676 23	+41 05 32.3113	10-03-2015	16 383	15.01	24.59	12 × 12
HD 45350	06 28 45.711 55	+38 57 46.6670	10-03-2015	50 000	15.01	75.05	12 × 12
Omi Uma	08 30 15.870 64	+60 43 05.4115	10-03-2015	20 000	5.01	10.02	12 × 12
GJ328	08 55 07.597	+01 32 56.44	10-03-2015	50 000	15.01	75.05	12 × 12
HD 95089	10 58 47.736 29	+01 43 45.1758	10-03-2015	32 766	15.01	49.18	12 × 12
HD 96063	11 04 44.454 63	−02 30 47.5867	10-03-2015	50 000	15.01	75.05	12 × 12
HD 99706	11 28 30.213 70	+43 57 59.6902	10-03-2015	50000	15.01	75.05	12 × 12
HD 100655	11 35 03.753 49	+20 26 29.5713	10-03-2015	50 000	15.01	75.05	12 × 12
HIP 57274	11 44 40.964 88	+30 57 33.4552	10-03-2015	50 000	15.01	75.05	12 × 12
HD 102329	11 46 46.645 18	+03 28 27.4563	10-03-2015	50 000	15.01	75.05	12 × 12
HD 106270	12 13 37.285 29	−09 30 48.1691	10-03-2015	16 383	15.01	24.59	12 × 12
HD 113337	13 01 46.926 69	+63 36 36.8092	10-03-2015	50 000	15.01	75.05	12 × 12
HD 116029	13 20 39.542 63	+24 38 55.3080	30-06-2013	50 000	29.54	147.70	24 × 24
	13 20 39.542 63	+24 38 55.3080	20-08-2014	60 000	29.54	177.24	24 × 24
HD 120084	13 42 39.201 86	+78 03 51.9756	10-03-2015	50 000	15.01	75.05	12 × 12
Beta UMi	14 50 42.325 80	+74 09 19.8142	10-03-2015	20 000	4	8.00	12 × 12
HD 131496	14 53 23.028 71	+18 14 07.4562	30-06-2013	50 000	29.54	147.70	24 × 24
	14 53 23.028 71	+18 14 07.4562	10-03-2015	50 000	15.01	75.05	12 × 12
HD 136726	15 17 05.888 99	+71 49 26.0466	30-06-2013	50 000	29.54	147.70	24 × 24
	15 17 05.888 99	+71 49 26.0466	10-03-2015	50 000	15.01	75.05	12 × 12
HD 136512	15 20 08.558 79	+29 36 58.3488	01-07-2013	50 000	29.54	147.70	24 × 24
	15 20 08.558 79	+29 36 58.3488	10-03-2015	50 000	15.01	75.05	12 × 12
HD 139357	15 35 16.198 86	+53 55 19.7129	01-07-2013	50 000	29.54	147.70	24 × 24
HD 145457	16 10 03.914 31	+26 44 33.8927	01-07-2013	50 000	29.54	147.70	24 × 24
HD 152581	16 53 43.582 57	+11 58 25.4822	01-07-2013	50 000	29.54	147.70	24 × 24
HAT-P-18	17 05 23.151	+33 00 44.97	30-06-2013	50 000	29.54	147.70	24 × 24
	17 05 23.151	+33 00 44.97	19-08-2014	65 540	29.54	193.61	24 × 24
	17 05 23.151	+33 00 44.97	20-08-2014	50 000	29.54	147.70	24 × 24
HD 156279	17 12 23.203 83	+63 21 07.5391	01-07-2013	50 000	29.54	147.70	24 × 24
HD 163607	17 53 40.494 79	+56 23 31.0417	30-06-2013	50 000	29.54	147.70	24 × 24
HD 163917	17 59 01.591 91	−09 46 25.0798	30-06-2013	50 000	29.54	147.70	24 × 24
HIP 91258	18 36 53.154 22	+61 42 09.0124	20-08-2014	50 000	29.54	147.70	24 × 24
Kepler-37	18 56 14.3063	+44 31 05.356	19-08-2014	50 000	29.54	147.70	24 × 24
Kepler-21	19 09 26.835 35	+38 42 50.4593	01-07-2013	50 000	29.54	147.70	24 × 24
	19 09 26.835 35	+38 42 50.4593	20-08-2014	50 000	29.54	147.70	24 × 24
HD 180314	19 14 50.208 90	+31 51 37.2569	30-06-2013	50 000	29.54	147.70	24 × 24
Kepler-63	19 16 54.294	+49 32 53.51	20-08-2014	50 000	29.54	147.70	24 × 24
Kepler-68	19 24 07.7644	+49 02 24.957	01-07-2013	50 000	29.54	147.70	24 × 24
	19 24 07.7644	+49 02 24.957	19-08-2014	50 000	29.54	147.70	24 × 24
Kepler-42	19 28 52.556	+44 37 09.62	30-06-2013	50 000	29.54	147.70	24 × 24
HAT-P-7	19 28 59.3616	+47 58 10.264	19-08-2014	50 000	29.54	147.70	24 × 24
HD 185269	19 37 11.740 92	+28 29 59.5055	30-06-2013	50 000	29.54	147.70	24 × 24
	19 37 11.740 92	+28 29 59.5055	19-08-2014	50 000	29.54	147.70	24 × 24
HD 188015	19 52 04.543 38	+28 06 01.3517	30-06-2013	50 000	29.54	147.70	24 × 24
	19 52 04.543 38	+28 06 01.3517	20-08-2014	50 000	29.54	147.70	24 × 24
HD 190360	20 03 37.405 87	+29 53 48.4944	01-07-2013	50 000	29.54	147.70	24 × 24

Table 1 – *continued*

Star	RA	Dec	Epoch	# of frames	Exposure time (ms)	Tot. integ. time (s)	Field of view (arcsec)
HD 197037	20 39 32.960 14	+42 14 54.7845	01-07-2013	50 000	29.54	147.70	24 × 24
	20 39 32.960 14	+42 14 54.7845	19-08-2014	50 000	29.54	147.70	24 × 24
HD 206610	21 43 24.900 04	−07 24 29.7086	20-08-2014	50 000	29.54	147.70	24 × 24
HD 208527	21 56 23.984 67	+21 14 23.4961	20-08-2014	50 000	29.54	147.70	24 × 24
HD 210277	22 09 29.865 52	−07 32 55.1548	19-08-2014	50 000	29.54	147.70	24 × 24
HD 217786	23 03 08.205	−00 25 46.66	28-07-2011	50 000	29.54	147.70	24 × 24
	23 03 08.205	−00 25 46.66	30-06-2013	50 000	29.54	147.70	24 × 24
	23 03 08.205	−00 25 46.66	20-08-2014	50 000	29.54	147.70	24 × 24
HD 240210	23 10 29.2303	+57 01 46.035	01-07-2013	50 000	29.54	147.70	24 × 24
HD 219828	23 18 46.734 45	+18 38 44.6021	30-06-2013	19 214	29.54	56.76	24 × 24
HD 220074	23 20 14.379 62	+61 58 12.4578	19-08-2014	50 000	29.54	147.70	24 × 24
HD 222155	23 38 00.307 41	+48 59 47.4907	01-07-2013	50 000	29.54	147.70	24 × 24

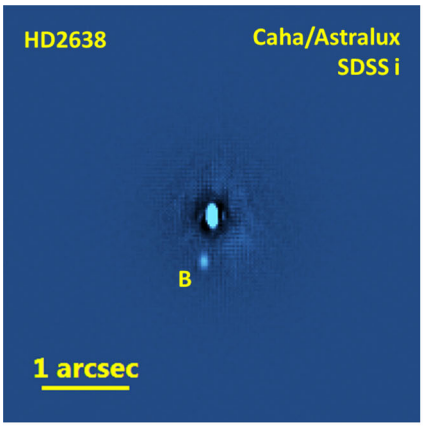

(a) HD 2638

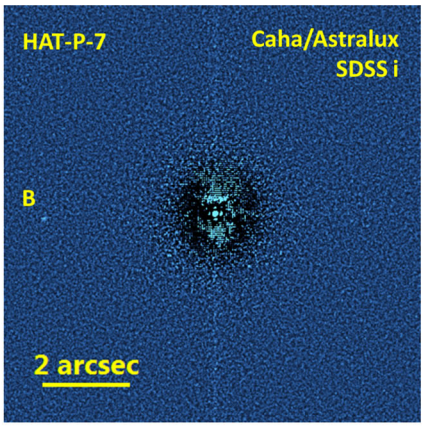

(b) HAT-P-7

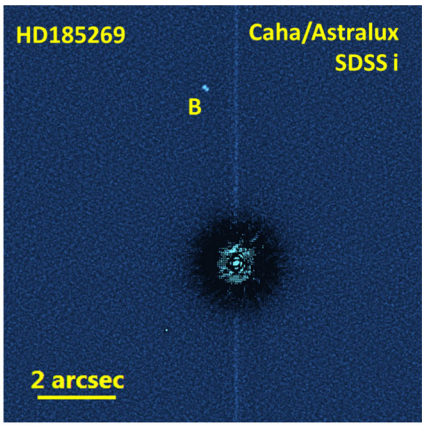

(c) HD 185269

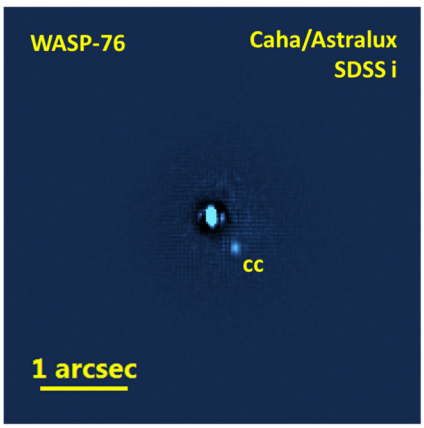

(d) WASP-76

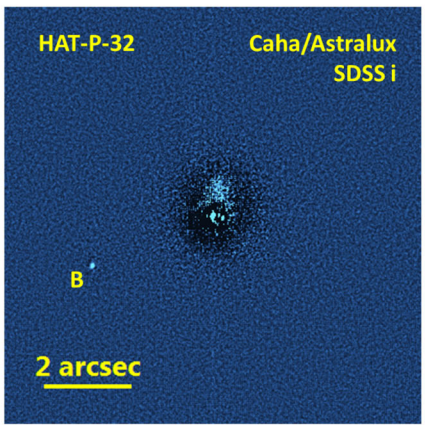

(e) HAT-P-32

Figure 1. Images of known low-mass stellar companions to exoplanet host stars, followed up in our multiplicity study. The haloes of the bright host stars were removed by high pass filtering. North is up and east is to the left.

primary star of the system. For this purpose, we are measuring the separation and relative position angle (PA) of all newly discovered companion candidates relative to the primary star. To ensure that our astrometric measurements can be compared between different observation epochs as well as with measurements done with different instrument, we took astrometric calibration images in each observation epoch. In 2013 and 2014, we used the centre of the globular cluster M 15 for this purpose. In the 2015 observation epoch M 15 was not visible and we imaged three wide binary systems instead (HIP 72508, HIP 80953 and HIP 59585). To calibrate the pixel scale as well as the orientation of the detector, we used as reference *HST* observations of M 15 that were taken on 2011-10-22 with the Wide Field Camera 3 (WFC3; Kimble et al. 2008). In the case of the binary stars, we used all measurements of the respective systems in the Washington Double Star Catalog (Mason et al. 2001) as reference. We applied a linear fit to these available measurements to correct for the slow orbital motion of these wide binaries. For the calibration using cluster data, we measured individual star

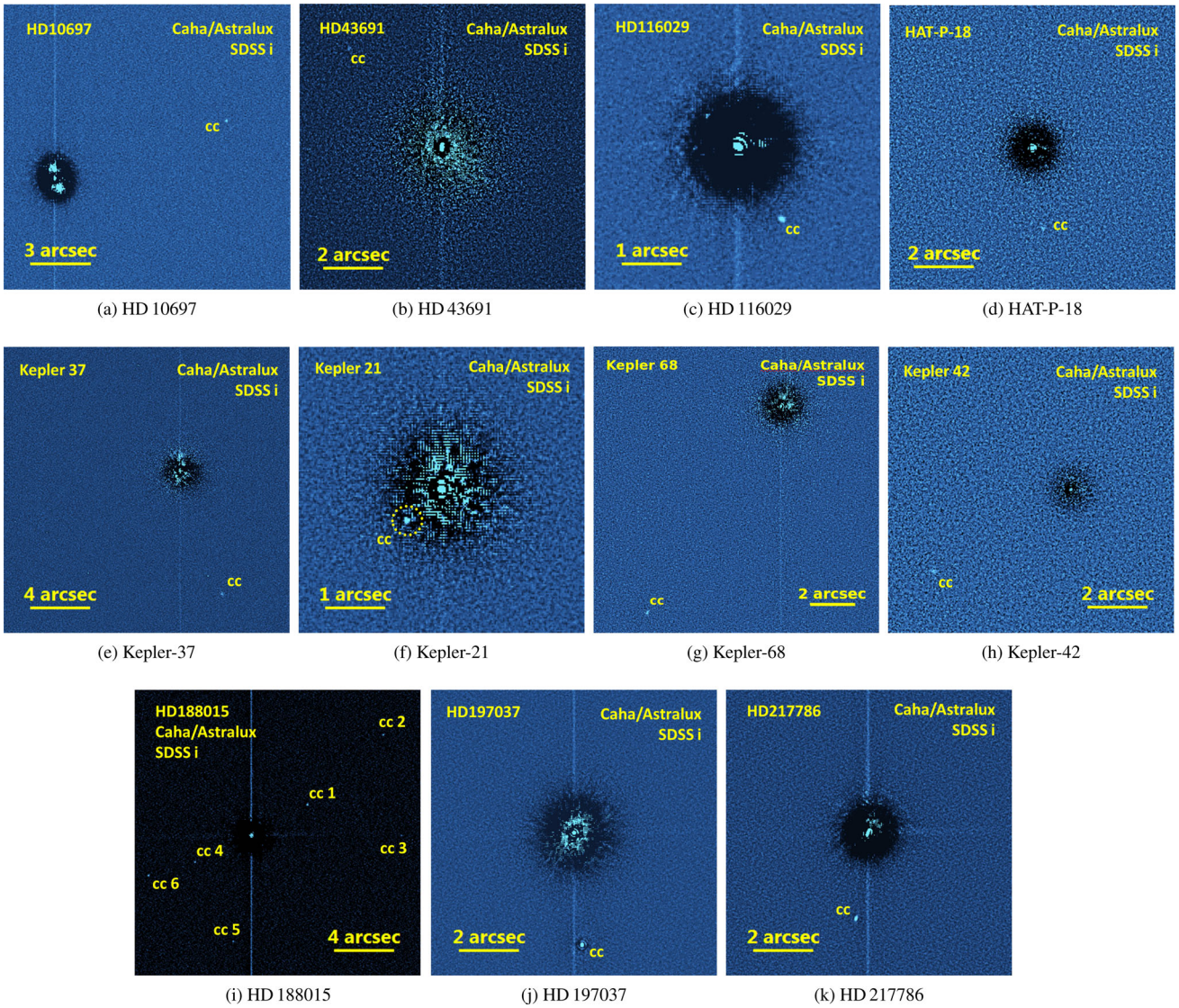

(a) HD 10697 (b) HD 43691 (c) HD 116029 (d) HAT-P-18

(e) Kepler-37 (f) Kepler-21 (g) Kepler-68 (h) Kepler-42

(i) HD 188015 (j) HD 197037 (k) HD 217786

Figure 2. Images of all newly detected companion candidates during the course of our multiplicity study with Astralux at the Calar Alto 2.2 m telescope. Spatial scaling of each image is indicated. The companion candidates (cc) are marked in all images. All images were high pass filtered to remove the bright halo of the host star. North is always up and east is to the left.

positions in our AstraLux image and the *HST* reference image with IDL[2] starfinder (Diolaiti et al. 2000), which fits a reference PSF to each star position. The reference PSF was created from the data itself. We then used our own cross-correlation routines to identify the same stars in both images. Finally, we calculated separations and relative orientations of each star relative to all other stars. This was done for 92 stars in 2013 and 90 stars in 2014. We then used the known astrometric calibration of the *HST* reference image to calculate an astrometric solution for each individual measurement. To exclude stars with a strong proper motion or possibly misidentified stars, we employed sigma clipping. The final astrometric solution for the 2013 and 2014 observations is the median of all computed solutions. We give the results in Table 2. The listed uncertainties are the standard deviations of all astrometric solutions.

In the case of the binary stars, we only have two objects in the field of view, thus we could not create a reference PSF from the data. Instead, we are fitting a two-dimensional Gaussian to the star positions. We checked that this approach is valid by comparing similar measurements in the cluster images with the starfinder results. The deviations between the two methods were typically much smaller than the measurement accuracy. The result of the binary calibration is also given in Table 2. We used the weighted average of the three solutions calculated from the individual binary systems. For the uncertainty, we conservatively assumed the largest individual uncertainty that we measured. The uncertainty of the calibration includes the uncertainty of the linear orbital motion fit mentioned earlier. We note that calibrations using binary stars are prone to systematic offsets due to unaccounted for (or underestimated) orbital motion of the systems. We thus caution that the result of the 2015 calibration might still suffer from such an offset.

We have one companion candidate which was already observed in July of 2011 for the first time. In this case, we utilized the astrometric calibration derived by us with cluster and binary data in Ginski et al. (2012).

For the SPHERE/IRDIS data, we used the astrometric solution calculated by the SPHERE consortium for the GTO run in which the

[2] Interactive Data Language.

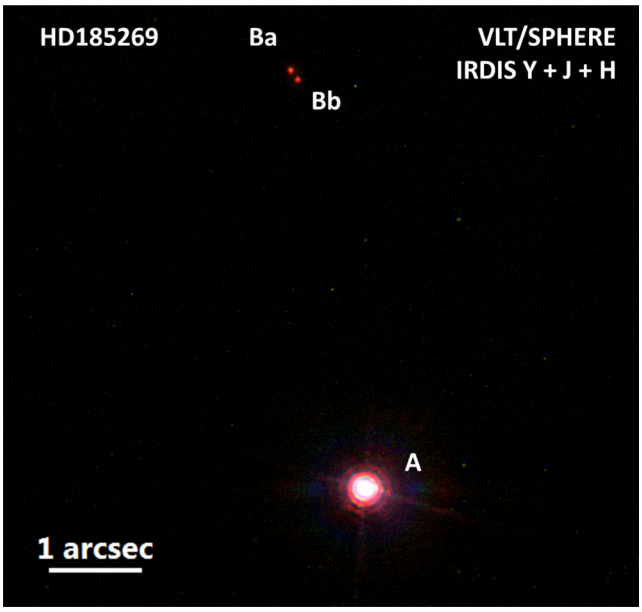

Figure 3. Composite colour image of the exoplanet host star HD 185269 and its companion taken with SPHERE/IRDIS on 2015-05-02. Red, green and blue channels are *H*, *J* and *Y* band data, respectively. In the SPHERE/IRDIS image the low-mass stellar companion discovered by us (Ginski et al. 2012) is for the first time resolved as a low-mass stellar binary. North is up and east is to the left.

Table 2. Astrometric calibration of all observation epochs as derived from observations of the centre of the globular cluster M 15. During our 2015 observation epoch M 15 was not visible; we instead used binary stars. We list the pixel-scale (PS) and the position angle (PA) of the *y*-axis for all observation epochs.

Epoch	PS (mas pix^{-1})	PA of *y*-axis (°)
30-06-2013	46.748 ± 0.14	358.18 ± 0.16
19-08-2014	46.864 ± 0.10	358.15 ± 0.12
10-03-2015	46.834 ± 0.13	357.66 ± 0.15

data were taken. This astrometric calibration was derived from multiple observations of the globular clusters 47 Tuc and NGC 6380, for which also precise *HST* reference observations as well as proper motions for individual cluster members are available. There is a small dependence of the pixel scale on the utilized filter; for our *Y*-band observations we used 12.234 ± 0.029 mas pix^{-1} and −1.78 ± 0.13 deg, while we used 12.214 ± 0.029 mas pix^{-1} for the *J* band, and 12.210 ± 0.029 mas pix^{-1} for the *H* band (the detector orientation is not influenced by the filter choice). In addition, IRDIS shows a small anamorphism between the detector *x* and *y* direction. This was also determined from observations of the globular cluster 47 Tuc. To correct for this anamorphism, we multiplied the separation in *y* by a factor of 1.0062. A detailed description of the IRDIS astrometric calibration is given in Maire et al. (2015).

The measurements of the relative positions of companion candidates to the primary stars was also done by fitting a two-dimensional Gaussian to both objects since there were no other objects in the field of view to build a reference PSF. Also, it is problematic to build an average reference PSF from different data sets, since the shape of the PSF will highly depend on the atmospheric conditions and the height of the target above the horizon. To ensure that we obtained a stable fitting result, we repeated the fitting procedure for each object at least 20 times with slightly different starting positions and fitting box sizes. For companion candidates that were separated by less than 2 arcsec from the bright primary stars, we removed the primary stars' bright halo by high pass filtering before we measured the companion candidates position. All results are listed in Table 3. The given uncertainties are the uncertainties of the Gaussian fitting added in quadrature to the uncertainties of the astrometric calibration. Multiple observation epochs were available for several systems. We discuss these systems in the following in detail and test if the companion candidates are comoving with the primary stars.

3.1 WASP-76

WASP-76 was observed by us only once in August of 2014. We detected a faint companion candidate ∼0.44 arcsec to the south-west of the star. Two months later in October of 2014, the target was observed also with AstraLux by Wöllert & Brandner (2015), who also detected this companion candidate and claim that it is likely a bound companion due to the decreasing likelihood of background objects with decreasing separation. We used their discovery astrometric data point, along with our own astrometric measurement, to determine if it is possible to draw conclusions on the proper motion of the object relative to the primary star. The corresponding diagram is shown in Fig. 4(a). In order to achieve an accurate position measurement of this faint source, we employed high pass filtering on the images to remove the bright halo of the exoplanet host.

Due to the short time baseline of only two months, and the large uncertainties given by Wöllert & Brandner (2015, presumably due to worse weather conditions compared with our own detection), it is not possible to draw firm conclusions on the proper motion of the companion candidate. However, we note that our own measurement is in principle more consistent with the object being a non-moving background source rather than a bound companion. Particularly the 1σ deviation of the two separation measurements could be well explained by parallactic displacement of the primary star relative to a presumably distant background source. Any future measurement with a similar precision as our own measurement of 2014 August will be enough to determine the status of this companion candidate.

3.2 HD 185269

A low-mass companion to the HD 185269 system was discovered by us with AstraLux observations in Ginski et al. (2012) with observations performed between 2008 and 2011. We followed up on this companion in our current study with observations taken in 2013 July and 2014 August. We show the image obtained in the 2013 observation epoch in Fig. 1. In this observation epoch, we observed for the first time that the companion appeared extended in north-east/south-west direction, while the PSF of the primary star showed no such distortion. This prompted us to re-observe this system with SPHERE/IRDIS. The much higher resolution extreme AO images of SPHERE show for the first time that the companion is actually a very low mass binary system itself with two approximately equally bright components (see Fig. 3). In addition to the (unresolved) follow-up astrometry performed with AstraLux, we measured the relative position of each binary component to the primary star in all bands of the SPHERE/IRDIS observation. We used again Gaussian fitting to determine the positions of all objects. The primary star shows a very mild saturation of the innermost 2–3 pixels in *Y* and *H* band. We measured its position again multiple times to ensure

Table 3. Relative astrometry and photometry of all detected known companions and new companion candidates extracted from our Astralux observations. We indicate if the companion candidate is comoving with the host star or not, if this can already be determined. We also give the confidence level of the proper motion result for the newly detected companion candidates, as well as the corresponding reference for the previously known systems.

Star	# cc	Epoch	Separation (arcsec)	Position angle (deg)	Δmag (mag)	Comoving?	Confidence level
			Known companions				
HD 2638		20-08-2014	0.5199 ± 0.0040	167.76 ± 0.35	3.11 ± 0.41	Yes	Roberts et al. (2015)
HAT-P-7		19-08-2014	3.828 ± 0.011	89.76 ± 0.20	7.556 ± 0.068	Yes	Narita et al. (2010)
HD 185269		30-06-2013	4.501 ± 0.016	8.09 ± 0.24	7.018 ± 0.067	Yes	Ginski et al. (2012)
		19-08-2014	4.533 ± 0.014	8.06 ± 0.22	7.118 ± 0.074		
WASP-76		20-08-2014	0.4438 ± 0.0053	214.92 ± 0.56	2.58 ± 0.27	–	Wöllert & Brandner (2015)
HAT-P-32		20-08-2014	2.9250 ± 0.0074	110.79 ± 0.17	5.403 ± 0.057	Yes	Ngo et al. (2015)
			New companion candidates				
HD 10697		21-08-2014	8.858 ± 0.019	286.73 ± 0.14	7.402 ± 0.095	–	
HD 43691		10-03-2015	4.435 ± 0.016	40.77 ± 0.24	7.71 ± 0.11	–	
HD 116029		30-06-2013	1.3871 ± 0.0058	209.11 ± 0.28	8.8 ± 1.8	–	
HAT-P-18		01-07-2013	2.643 ± 0.014	185.72 ± 0.33	7.19 ± 0.12	–	
Kepler-37		20-08-2014	8.516 ± 0.019	196.93 ± 0.15	6.347 ± 0.056	No	4.3σ
Kepler-21		02-07-2013	0.7671 ± 0.0062	129.74 ± 0.46	$5.9^{+4.2}_{-1.0}$	Yes	4.0σ
		20-08-2014	0.7739 ± 0.0099	129.53 ± 0.63	<8.1		
Kepler-68		02-07-2013	10.953 ± 0.034	145.39 ± 0.20	6.569 ± 0.073	Yes	2.1σ
		19-08-2014	10.979 ± 0.030	145.43 ± 0.18	6.641 ± 0.075		
Kepler-42		01-07-2013	5.206 ± 0.017	118.93 ± 0.21	4.157 ± 0.082	–	
HD 188015	1	01-07-2013	4.167 ± 0.013	296.88 ± 0.20	8.46 ± 0.12	No	3.0σ
	2	01-07-2013	10.835 ± 0.033	305.61 ± 0.19	9.00 ± 0.15	–	
	3	01-07-2013	9.784 ± 0.031	268.09 ± 0.20	9.40 ± 0.18	–	
	4	01-07-2013	4.063 ± 0.013	113.72 ± 0.20	9.05 ± 0.15	–	
	5	01-07-2013	7.037 ± 0.021	168.55 ± 0.19	9.35 ± 0.18	–	
	6	01-07-2013	7.197 ± 0.022	109.60 ± 0.19	8.78 ± 0.14	–	
	1	20-08-2014	4.237 ± 0.014	297.52 ± 0.22	8.91 ± 0.23		
	2	20-08-2014	10.9449 ± 0.070	305.71 ± 0.37	9.11 ± 0.23		
	3	20-08-2014	9.947 ± 0.102	268.15 ± 0.52	9.47 ± 0.29		
	4	20-08-2014	4.006 ± 0.067	112.48 ± 0.79	9.25 ± 0.36		
	6	20-08-2014	7.066 ± 0.068	109.41 ± 0.50	8.78 ± 0.18		
HD 197037		02-07-2013	3.676 ± 0.011	182.21 ± 0.18	5.124 ± 0.051	Yes	19.2σ
		20-08-2014	3.6876 ± 0.0088	182.14 ± 0.17	5.159 ± 0.052		
HD 217786		28-07-2011	2.8105 ± 0.0091	170.81 ± 0.26	7.212 ± 0.078	Yes	46.8σ
		01-07-2013	2.8327 ± 0.0092	170.22 ± 0.20	7.171 ± 0.084		
		21-08-2014	2.8560 ± 0.0069	170.34 ± 0.16	7.160 ± 0.096		

that we reached a good fit (we fit the flanks of the saturated PSF in this case). Final results are listed in Table 4. In addition, we used our measurements to calculate the weighted average of the position of the Bb component with respect to the Ba component. We arrive at a separation of 123.55 ± 0.44 mas (∼5 au projected separation at a distance of 47.37 ± 1.72 pc; van Leeuwen 2007) and a PA of 214.87 ± 0.21 deg.

Since the SPHERE image confirmed that HD 185269 B is a binary, we re-examined our 2013 AstraLux observation in order to provide an astrometric measurement of the relative binary position. This is useful to determine the orbit of the binary and constrain its mass dynamically in later follow-up studies of the system. Due to the marginally resolved nature of the binary source in our 2013 AstraLux data, Gaussian fitting proved to be difficult. Instead, we used the primary star's PSF as template and fitted it to the two components of HD 185269 B using IDL starfinder. This fit yielded a separation of 95.6 ± 2.8 mas and a PA of 221.1 ± 1.3 deg of Bb relative to Ba, as well as separations of 4538 ± 14 mas and 4458 ± 14 mas and PAs of 8.39 ± 0.17 deg and 7.72 ± 0.18 deg of Ba and Bb relative to A. As expected for a system with such small separation, we see strong orbital motion between the 2013 and the 2015 observation epoch. Due to the non-optimal weather conditions in 2014, the companion is not resolved in our 2014 AstraLux observation. At least one additional astrometric measurement is needed to constrain the orbital elements of this binary system.

3.3 HD 43691

HD 43691 was imaged by us once in March of 2015. We detected a companion candidate approximately 4.4 arcsec to the north-east of the exoplanet host star. Since we only have one epoch it is not yet possible to determine if the object is indeed related to the HD 43691 system. However, upon close inspection of the companion candidate's PSF we noticed that it appears extended along an angle of roughly 135 deg. A close-up of the companion candidate's PSF, as well as the primary stars' PSF, is shown in Fig. 5. We actually see at least two distinct peaks in the PSF (signal-to-noise ratio[3] of 5.8 and 5.5, separation of ∼84 mas, i.e. 6.7 au at 80.4 pc), which would indicate that the object itself may be a multiple system. We compared the companion candidate's PSF with the PSF of the primary star

[3] The noise was determined by calculating the standard deviation in a 5 × 5 pixel box centred on the two brightest peaks of the source.

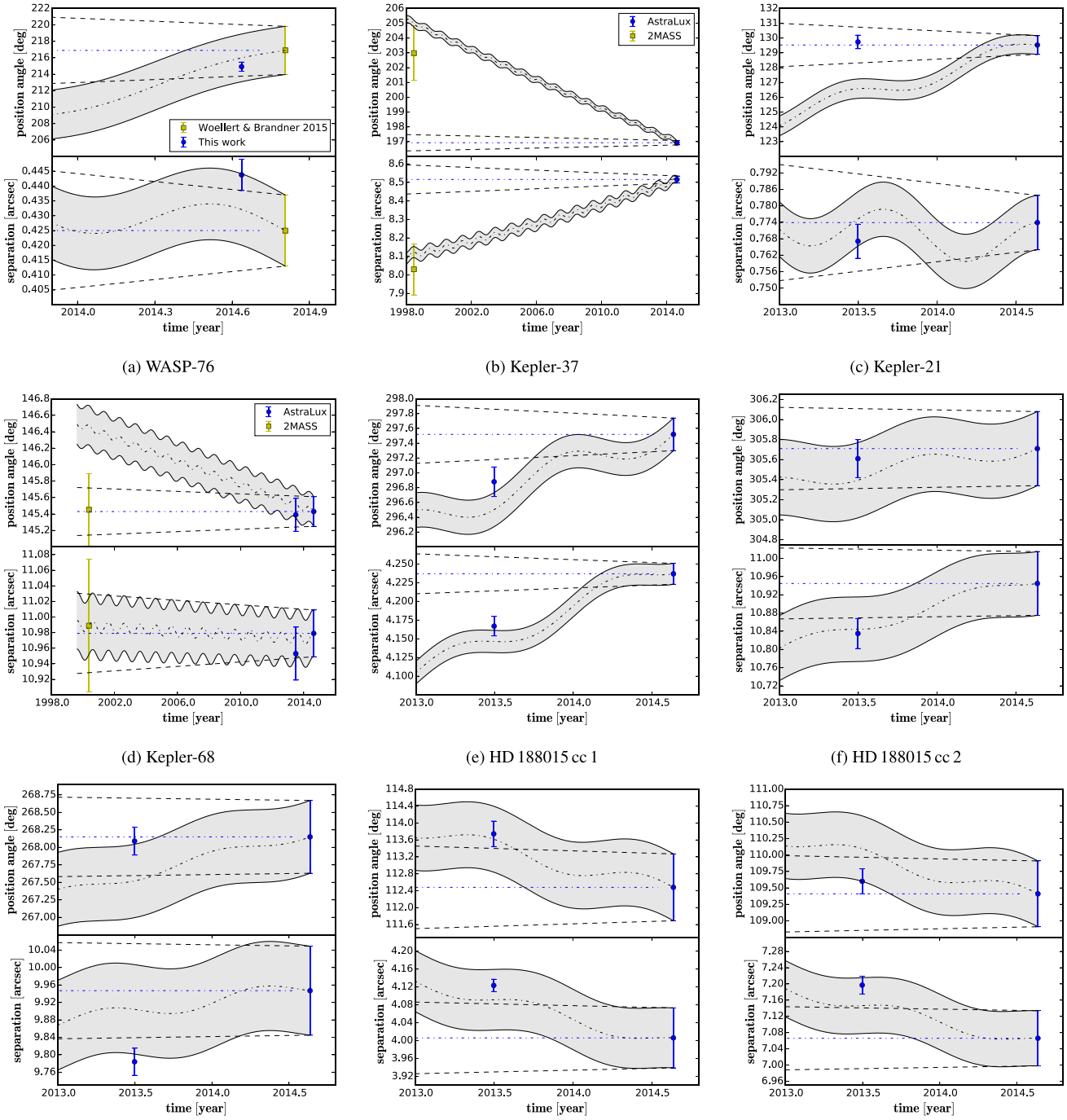

(a) WASP-76 (b) Kepler-37 (c) Kepler-21

(d) Kepler-68 (e) HD 188015 cc 1 (f) HD 188015 cc 2

(g) HD 188015 cc 3 (h) HD 188015 cc 4 (i) HD 188015 cc 6

Figure 4. Proper motion analysis for all companion candidates with two or more observation epochs. Data points are AstraLux measurements if not otherwise marked. The dashed lines enclose the area in which a comoving companion would be expected. This takes into account possible circular orbital motion with the semimajor axis given by the projected separation of the companion. The grey area enclosed by the wobbled lines is the area in which a non-moving background object would be expected, depending on the proper motion and distance of the primary star. The wobble is introduced by the parallactic shift in the primary position due to the Earth's revolution around the sun.

to exclude that this is merely an effect caused by the observation conditions. However, the primary star' PSF appears circular in the centre with a halo that is slightly extended in north–south direction, i.e. we see no indication for an intrinsic smearing of the PSF along the angle seen in the companion candidate. We note that there appears to be a third peak directly north of the south-east component of the companion candidate's PSF. This might indeed be a residual of a north–south extended halo, as seen in the primarie's PSF. The object might hence be a binary or even trinary companion to HD 43691 A. However, further observations are required to confirm that the source is comoving with the primary star and that it is indeed a multiple system itself.

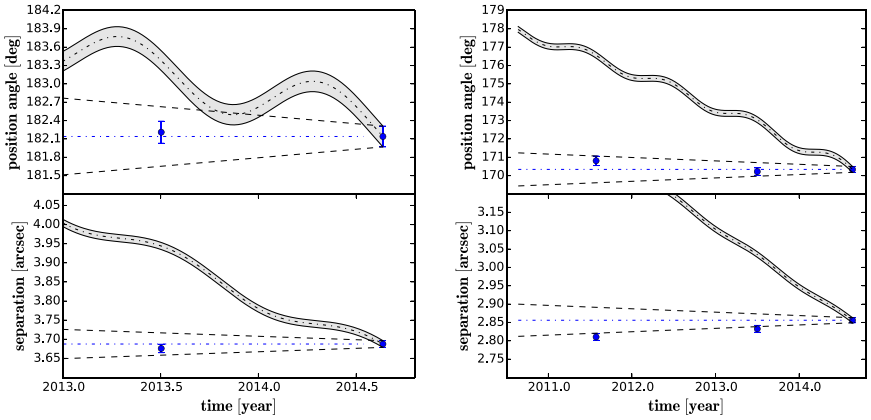

(j) HD 197037 (k) HD 217786

Figure 4 *– continued.*

Table 4. Astrometric measurements of the two low-mass binary components of the HD 185269 system relative to the host star from SPHERE data.

	Ba		Bb	
Filter	Sep. (arcsec)	PA (°)	Sep. (arcsec)	PA (°)
Y	4.549 ± 0.011	8.15 ± 0.15	4.442 ± 0.011	7.43 ± 0.14
J	4.547 ± 0.011	8.15 ± 0.14	4.436 ± 0.011	7.44 ± 0.15
H	4.547 ± 0.011	8.15 ± 0.15	4.436 ± 0.011	7.43 ± 0.15

3.4 Kepler-37

Kepler-37 (KOI-245, KIC 8478994) was observed by us only once in August of 2014. In this data set we discovered a wide (∼8.5 arcsec) companion candidate south-south-west of the exoplanet host star. Kepler-37 was previously observed by Lillo-Box, Barrado & Bouy (2014), also using AstraLux at the Calar Alto observatory. In addition, it was targeted by Adams et al. (2012) using ARizona Infrared imager and Echelle Spectrograph (ARIES) at the Multiple Mirror Telescope (MMT) observatory. Both studies do not mention the companion candidate recovered in our own AstraLux image, since they are focusing on close companions within 6 arcsec of the primary star.

Since the object was located at such a relatively large separation, we decided to check the 2MASS (Skrutskie et al. 2006) survey for previous detection. While the object was not listed in the 2MASS point source catalogue, it was visible in the reduced *J*, *H* and *K* images. We extracted the astrometric position from the individual 2MASS images using Richardson–Lucy deconvolution and then averaged the results over all bands. For details on the extraction, we refer to our recent study Mugrauer & Ginski (2015). We find a separation of 8.030 ± 0.138 arcsec and a PA of 202.99 ± 1.85 deg in the 2MASS observation epoch of 1998.47. We used the 2MASS data in combination with our more precise AstraLux measurement to test if the discovered object is comoving with the primary star. The corresponding diagram is shown in Fig. 4(b). Even though the uncertainties of the 2MASS measurement are large compared to our AstraLux measurement, the position of the companion candidate in the 2MASS epoch is consistent within 1σ with a non-moving background object. By comparison, co-motion with the primary can be rejected on the 4σ level. We thus conclude that the object is likely located in the distant background and is not physically associated with the Kepler-37 system.

3.5 Kepler-21

Kepler-21 (KOI-975, KIC 3632418) was observed in July of 2013 and August 2014 with Astralux. A very close companion candidate at approximately 0.8 arcsec was detected south-east of the primary star. In order to get an accurate position measurement of this faint source, we employed high pass filtering on the images to remove the bright halo of the exoplanet host. The resulting measurements were compared with the proper motion of the primary star. The corresponding diagram is shown in Fig. 4(c). Due to the direction of motion of Kepler-21, no significant change in separation would be expected for a comoving object as well as a non-moving background object. However, as can be seen in the diagram, both types of objects diverge in expected PA. Our measurements of the PA of the companion candidate show no significant change in PA, consistent with common proper motion. We can reject the background hypothesis with 4.0σ. We thus conclude that the object that we detected is most likely gravitationally bound to Kepler-21 A and is thus a new low-mass stellar companion in this system.

3.6 Kepler-68

Kepler-68 (KOI-246, KIC 11295426) was imaged by us also in July of 2013 and August of 2014. A wide companion candidate approximately 11 arcsec to the south-east was detected in both observation epochs. Unfortunately Kepler-68 exhibits only a very small proper motion of -10.60 ± 1.60 mas yr^{-1} in declination and -8.50 ± 1.60 mas yr^{-1} in right ascension. Thus with only one year of epoch difference it was not possible to assert whether the companion candidate is comoving with the primary star. However, since the companion candidate is located at a wide separation, we checked again the 2MASS catalogue to see if the source had been previously detected. We found that our companion candidate is indeed contained in the 2MASS point source catalogue at a relative position of 10.989 ± 0.085 arcsec and 145.45 ± 0.44 deg. Using this additional observation epoch, we tested the companion for common proper motion with the primary star. The corresponding diagram is shown in Fig. 4(d). While the separation is inconclusive due to the tangential direction of motion of the primary star, we would have expected a significant change in PA of our measurements with respect to the 2MASS epoch if the companion candidate was a non-moving background object. Instead, we find that all measurements are consistent with no change in PA. However, due to the large

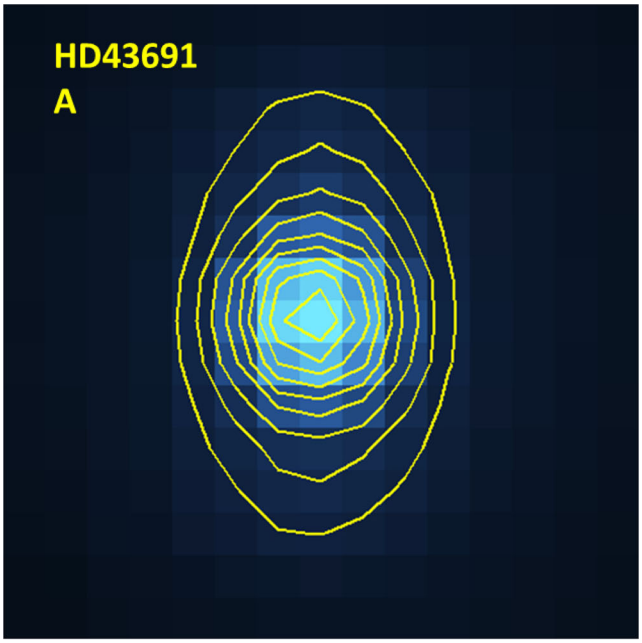

(a) HD 43691 A

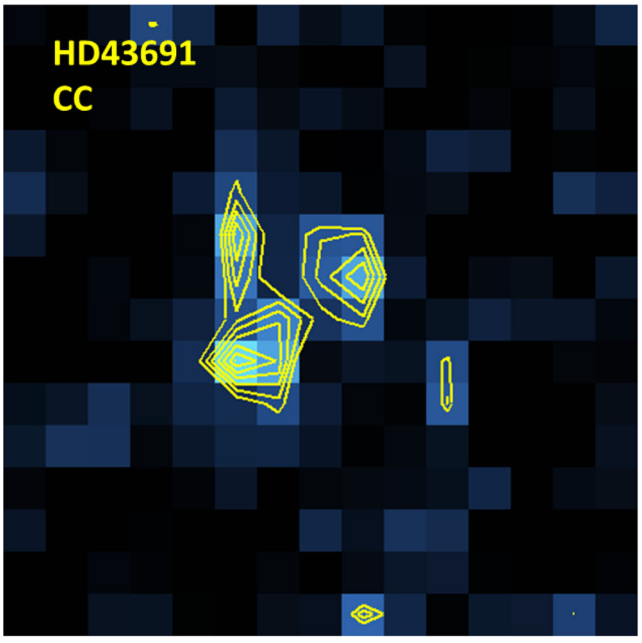

(b) HD 43691 cc

Figure 5. Close-up of the primary star and companion candidate PSF of HD 43691. The primary star appears relatively circular with a halo that extends in the north–south direction. The companion candidate shows at least two distinct brightness peaks that are extending at an angle of approximately 135 deg. Contour lines have been overplotted to guide the eye.

uncertainties of the 2MASS epoch we can only reject the background hypothesis with 2.1σ. We conclude that, given our data, it seems likely that the companion candidate is indeed bound to the Kepler-68 system, but further observations need to be undertaken to strengthen this conclusion.

3.7 HD 188015

HD 188015 was observed by us with AstraLux in 2013 July and 2014 August. In Fig. 2(i), we show our 2013 observation epoch. A total of six companion candidates are visible in the field of view of AstraLux. The high density of objects in the field of view compared to other systems is not entirely surprising since HD 188015 is located in the direction of the Galactic disc (Galactic latitude of $+00\overset{\circ}{.}5428$). We note that HD 188015 has a known low-mass stellar companion at ∼13 arcsec and a PA of 85 deg, discovered by Raghavan et al. (2006) in Sloan Digital Sky Survey (SDSS; York et al. 2000) data. This companion is outside of the field of view of our AstraLux observations.

In 2014 August observation conditions were not as favourable as in 2013 with shorter coherence times and thin cloud layers passing through during the observations. Thus only the candidate marked as cc1 was re-detected with high signal to noise. Of the other five companions, four were detected marginally with cc5 being the exception. The marginal detections in 2014 did not allow for fitting of a Gaussian to the companion candidates. Instead, we have determined the centre of light with a simple centroid for those four sources. This led to much larger uncertainties of the 2014 astrometry. We none the less used the 2014 astrometry in combination with the known proper motion of the primary star to determine if one or several of the companion candidates are comoving with the primary star. The corresponding diagrams for cc1 to cc6 (with the exception of cc5) are shown in Fig. 4(e)–Fig. 4(i). For cc1, the available astrometry is more consistent with a background object and we can reject common proper motion with HD 188015 A on the 3σ level. For the remaining companion candidates we cannot reject common proper motion or background hypothesis with any significance. This is caused by the larger uncertainty of the 2014 measurements in combination with the short time baseline of only one year. We note, however, that the astrometry of cc2 and cc4 is more consistent with a distant background object, while the same is not true for cc3 and cc6. The latter two remain completely inconclusive due to their opposite behaviour in separation and PA. We point out that this seemingly mixed behaviour could be caused by a non-zero proper motion of these objects. To gain a better understanding of this system, at least one further observation epoch in good observing conditions is required.

3.8 HD 197037

HD 19037 was observed by us with AstraLux in two epochs in 2013 July and 2014 August. We detected a companion candidate approximately 3.7 arcsec to the south of the primary star. Using the proper motion of the primary star, we calculated the expected position of a non-moving background object in 2013 given the 2014 measurement. The corresponding diagram is shown in Fig. 4(j). The astrometry in both epochs is consistent with no significant change in relative position. We can reject the background hypothesis with 4.8σ in separation and 18.6σ in PA. We conclude that the detected object is comoving with HD 19037 A and is thus most likely a new gravitationally bound stellar companion to the system.

3.9 HD 217786

HD 217786 was observed by us on three different occasions in 2011 and 2013 July, as well as in August of 2014. In all three observation epochs, we detected a companion candidate approximately 2.8 arcsec to the south of the primary star. The proper motion for this

system is well determined to be -88.78 ± 0.84 mas yr^{-1} in declination and -170.13 ± 0.61 mas yr^{-1} in right ascension (van Leeuwen 2007). We show the astrometric measurements as well as the expected behaviour of a background object in Fig. 4(k). The PA of the companion candidate is not changing significantly with time. However, we detect a small increase in separation. The dashed lines in the diagram show the expected change for a circular edge-on orbit. The data points are consistent with such a change within 1σ. We note that even stronger changes in separation are possible for eccentric orbits. The change in separation is much smaller than what would be expected from a background object and is also showing the wrong direction (for a background object the separation should have decreased from 2011 to 2014). In fact, we can reject the background hypothesis with 42.8σ in separation and 18.9σ in PA. We thus conclude that the discovered object is very likely bound to the system and emerges as new low-mass stellar companion. Due to the small change in separation, but no change in PA, we expect the companion to be in a close to edge-on orbit configuration, but longer astrometric monitoring is required to test this hypothesis.

4 PHOTOMETRIC MEASUREMENTS AND MASS DETERMINATION

To determine the masses of the confirmed companions as well as the possible companion candidates, we performed photometric measurements for all our observation epochs. Since the photometry depends on the gain settings of the detector as well as the observation conditions and height of the target, we did not record a photometric standard star and rather give relative photometric measurements of the companions (and candidates) to their primary stars. While the PSFs of all sources in one image are similar, they are changing with observing conditions and elevation of the targets as well, thus it is not possible to build a reference PSF for photometric measurements from the data. We instead decided to perform aperture photometry on all sources. We used the aperture photometry tool (Laher et al. 2012) for these measurements. The aperture size was adjusted for each image individually to encircle the majority of the flux of the companion candidates. The same aperture size was then used to get the reference measurement from the primary star. In the cases where the faint sources were located within the bright halo of the primary star, care was taken to select a sky aperture close to the companion position to accurately subtract the contribution of the primary to the flux in the aperture. In the case of the primary star, we used sky apertures with large separations from the primary in order to not oversubtract flux due to halo contributions. All results are given in Table 3.

The presented uncertainties take into account statistical uncertainties, which were scaled with a factor of $\sqrt{2}$ to take into account the increased photometric uncertainty of electron multiplying CCDs. In addition, we consider uncertainties in the differential magnitudes from changing aperture sizes, i.e. if we increase or decrease the aperture radius by up to 2 pixels. These were typically in the order of 0.04 mag and were added in quadrature to the statistical uncertainties.

To convert our photometric measurements to masses we used the BT-SETTL evolutionary models for low-mass stars, brown dwarfs and planets (Allard, Homeier & Freytag 2011). These models take the absolute magnitude and the age of an object as input. To compute the absolute magnitude of our confirmed/possible companions we used the apparent magnitude of the host star in the SDSS *i* band, as well as the distance of the host star. We then assume that the companions are of the same age as the host star. We summarize these input values for all targets in our survey in Table 5. To get a finer model-grid we interpolated (linearly) between different model ages and star magnitudes. The final masses for all confirmed or possible companion candidates are listed along with their derived absolute magnitude in Table 6. The listed uncertainties for the absolute magnitude include the uncertainty of the apparent magnitude of the host star, as well as the uncertainty in the measured differential magnitude and the uncertainty in the distance of the system. The uncertainties listed for the masses of the objects also account for the uncertainty of the system age. In the following, we compare our photometric measurements and mass determination for a few systems with available literature values.

4.1 HD 2638

For the close stellar companion to HD 2638, we find a differential magnitude of 3.11 ± 0.41 mag in the SDSS *i* band. Using this measurement along with the age, distance and apparent magnitude of the primary star, we find a mass of $0.425^{+0.067}_{-0.095}$ $M_\odot$ for the companion. The companion was originally discovered by Riddle et al. (2015) using Robo-AO in the optical. They have two measurements in the SDSS *i* band and find differential magnitudes between primary and companion of 3.39 and 3.19 mag (Riddle et al. 2015; Roberts et al. 2015). They do not provide uncertainties for these measurements. However, given our own uncertainties, both values are within 1σ of our own measurement. To compare our mass result with independent measurements, we used the K_s and *J*-band photometric measurements of the companion, provided in the characterization paper of the object by Roberts et al. (2015). To calculate a mass range we use again BT-SETTL models. We find an approximate mass range of 0.53 $M_\odot$–0.45 $M_\odot$. While this is slightly larger than our own SDSS *i*-band result, both measurements are consistent within our 1σ uncertainties. The small discrepancy might be explained by a potential oversubtraction of background flux in our SDSS *i*-band images.

4.2 HAT-P-7

We measure a differential SDSS *i*-band magnitude between HAT-P-7 A and B of 7.556 ± 0.068 mag. This value is in excellent agreement with the measurement very recently reported in Wöllert et al. (2015), who use the same instrument setup and find a value of 7.58 ± 0.17 mag. Using our differential SDSS *i*-band magnitude and the system parameters listed in Table 5, we arrive at a mass of $0.205^{+0.026}_{-0.021}$ $M_\odot$. This mass estimate is consistent with the mass range given in the discovery paper by Narita et al. (2010), who find 0.17–0.20 $M_\odot$ from near-infrared and optical photometry. It also agrees with the more recent mass estimated by Ngo et al. (2015), who find a range of 0.196–0.232 $M_\odot$, also from near-infrared photometry.

4.3 HD 185269

The photometric measurements in SDSS *i* band of the 2013 and 2014 AstraLux observation of this system are consistent within 1σ with the previous value published by us in Ginski et al. (2012). Besides the unresolved SDSS *i*-band photometry, the SPHERE data enabled us to take photometric measurements of the individual components of HD 185269 B. Since we do not have additional sources in the field of view other than the primary and the binary companion, we again used aperture photometry to derive the brightness of the binary

Table 5. Distances, apparent magnitudes and ages of all target stars in our survey. We give the corresponding references in adjacent columns.

Star	SDSS *i* (mag)	Ref.	Distance (pc)	Ref.	Age (Gyr)	Ref.
HD 2638	9.01 ± 0.03	Ofek (2008)	49.9 ± 4.0	van Leeuwen (2007)	1.9 ± 2.6	Bonfanti et al. (2015)
HD 2952	–		114.2 ± 6.2	van Leeuwen (2007)	–	
HD 5608	5.49 ± 0.03	Ofek (2008)	56.4 ± 1.3	van Leeuwen (2007)	–	
HD 5891	7.474 ± 0.01	Ahn et al. (2012)	251.3 ± 109.8	van Leeuwen (2007)	1.5 ± 0.1	Bonfanti et al. (2015)
HD 8574	6.97 ± 0.01	Ofek (2008)	44.6 ± 1.1	van Leeuwen (2007)	5.0 ± 0.1	Bonfanti et al. (2015)
HD 10697	5.91 ± 0.15	Ofek (2008)	32.6 ± 0.5	van Leeuwen (2007)	7.1 ± 0.1	Bonfanti et al. (2015)
WASP-76	9.318 ± 0.001	Ahn et al. (2012)	120.0 ± 20.0	West et al. (2016)	$5.3^{+6.1}_{-2.9}$	West et al. (2016)
HAT-P-32	11.12 ± 0.08	Ofek (2008)	320.0 ± 16.0	Hartman et al. (2011b)	0.1 ± 0.1	Bonfanti et al. (2015)
HD 12661	7.1 ± 0.04	Ofek (2008)	35.0 ± 0.8	van Leeuwen (2007)	1.8 ± 0.5	Bonfanti et al. (2015)
HD 13189	6.56 ± 0.09	Ofek (2008)	561.8 ± 390.6	van Leeuwen (2007)	–	
HD 13908	7.33 ± 0.02	Ofek (2008)	71.2 ± 3.7	van Leeuwen (2007)	2.9 ± 0.4	Moutou et al. (2014)
HD 15779	4.82 ± 0.04	Ofek (2008)	81.4 ± 3.1	van Leeuwen (2007)	–	
HD 285507	9.91 ± 0.11	Ofek (2008)	41.3 ± 4.0	van Leeuwen (2007)	0.63 ± 0.05	Quinn et al. (2014)
HD 290327	8.62 ± 0.03	Ofek (2008)	56.7 ± 5.5	van Leeuwen (2007)	11.8 ± 1.2	Bonfanti et al. (2015)
HD 40979	6.57 ± 0.02	Ofek (2008)	33.1 ± 0.5	van Leeuwen (2007)	1.5 ± 0.5	Mugrauer et al. (2007)
HD 43691	7.88 ± 0.02	Ofek (2008)	80.4 ± 5.7	van Leeuwen (2007)	3.1 ± 2.5	Bonfanti et al. (2015)
HD 45350	7.53 ± 0.03	Ofek (2008)	48.9 ± 1.8	van Leeuwen (2007)	7.0 ± 0.9	Bonfanti et al. (2015)
Omi Uma	2.9635 ± 0.042	Jester et al. (2005)	54.9 ± 0.5	van Leeuwen (2007)	0.36 ± 0.03	Soubiran et al. (2008)
GJ328	8.946 ± 0.131	Jester et al. (2005)	19.8 ± 0.8	Robertson et al. (2013)	–	
HD 95089	7.4 ± 0.03	Ofek (2008)	139.1 ± 18.2	van Leeuwen (2007)	2.3 ± 0.2	Bonfanti et al. (2015)
HD 96063	7.76 ± 0.04	Ofek (2008)	158.0 ± 23.5	van Leeuwen (2007)	3.6 ± 0.7	Bonfanti et al. (2015)
HD 99706	7.14 ± 0.03	Ofek (2008)	128.9 ± 12.4	van Leeuwen (2007)	2.8 ± 0.2	Bonfanti et al. (2015)
HD 100655	5.93 ± 0.11	Ofek (2008)	122.2 ± 8.0	van Leeuwen (2007)	0.9 ± 0.2	Bonfanti et al. (2015)
HIP 57274	8.23 ± 0.03	Ofek (2008)	25.9 ± 0.7	van Leeuwen (2007)	8.4 ± 3.7	Bonfanti et al. (2015)
HD 102329	7.32 ± 0.02	Ofek (2008)	158.0 ± 23.8	van Leeuwen (2007)	2.0 ± 0.3	Bonfanti et al. (2015)
HD 106270	7.21 ± 0.04	Ofek (2008)	84.9 ± 6.1	van Leeuwen (2007)	4.0 ± 0.1	Bonfanti et al. (2015)
HD 113337	5.95 ± 0.02	Ofek (2008)	36.9 ± 0.4	van Leeuwen (2007)	0.2 ± 0.1	Borgniet et al. (2014)
HD 116029	7.36 ± 0.04	Ofek (2008)	123.2 ± 10.7	van Leeuwen (2007)	3.5 ± 0.5	Bonfanti et al. (2015)
HD 120084	5.37 ± 0.05	Ofek (2008)	100.7 ± 2.5	van Leeuwen (2007)	1.1 ± 0.3	Soubiran et al. (2008)
Beta UMi	1.081 ± 0.042	Jester et al. (2005)	40.1 ± 0.2	van Leeuwen (2007)	3.0 ± 1.0	Lee et al. (2014)
HD 131496	7.33 ± 0.03	Ofek (2008)	110.0 ± 10.3	van Leeuwen (2007)	4.5 ± 0.4	Bonfanti et al. (2015)
HD 136726	4.25 ± 0.06	Ofek (2008)	122.1 ± 2.9	van Leeuwen (2007)	3.9 ± 0.9	Bonfanti et al. (2015)
HD 136512	4.99 ± 0.06	Ofek (2008)	82.8 ± 3.1	van Leeuwen (2007)	5.6 ± 2.2	Soubiran et al. (2008)
HD 139357	4.68 ± 0.5	Monet et al. (2003)	118.1 ± 4.3	van Leeuwen (2007)	7.0 ± 2.0	Bonfanti et al. (2015)
HD 145457	6.08 ± 0.11	Ofek (2008)	125.3 ± 7.5	van Leeuwen (2007)	2.6 ± 0.4	Bonfanti et al. (2015)
HD 152581	7.95 ± 0.03	Ofek (2008)	185.5 ± 40.2	van Leeuwen (2007)	8.6 ± 2.1	Bonfanti et al. (2015)
HAT-P-18	12.125 ± 0.01	Abazajian et al. (2009)	166.0 ± 9.0	Hartman et al. (2011a)	12.4 ± 6.4	Hartman et al. (2011a)
HD 156279	7.65 ± 0.03	Ofek (2008)	36.6 ± 0.6	van Leeuwen (2007)	7.4 ± 1.9	Bonfanti et al. (2015)
HD 163607	7.643 ± 0.001	Ahn et al. (2012)	68.8 ± 2.3	van Leeuwen (2007)	8.91 ± 0.01	Bonfanti et al. (2015)
HD 163917	2.78 ± 0.03	Ofek (2008)	46.2 ± 0.6	van Leeuwen (2007)	0.45 ± 0.07	Soubiran et al. (2008)
HIP 91258	8.33 ± 0.02	Ofek (2008)	44.9 ± 1.4	van Leeuwen (2007)	2.4 ± 2.4	Moutou et al. (2014)
Kepler-37	9.38 ± 0.04	Ofek (2008)	66.0 ± 33.0	Barclay et al. (2013)	3.7 ± 0.8	Walkowicz & Basri (2013)
Kepler-21	8.06 ± 0.03	Ofek (2008)	112.9 ± 7.9	van Leeuwen (2007)	3.55 ± 0.03	Bonfanti et al. (2015)
HD 180314	6.14 ± 0.05	Ofek (2008)	131.4 ± 7.1	van Leeuwen (2007)	0.9 ± 0.6	Bonfanti et al. (2015)
Kepler-63	11.44 ± 0.02	Zacharias et al. (2013)	200.0 ± 15.0	Sanchis-Ojeda et al. (2013)	0.210 ± 0.045	Sanchis-Ojeda et al. (2013)
Kepler-68	9.83 ± 0.02	Ofek (2008)	135.0 ± 10.0	Gilliland et al. (2013)	6.3 ± 1.7	Gilliland et al. (2013)
Kepler-42	14.375 ± 0.5	Zacharias et al. (2013)	38.7 ± 6.3	Muirhead et al. (2012)	5.0 ± 1.0	Muirhead et al. (2012)
HAT-P-7	10.37 ± 0.01	Ofek (2008)	320.0 ± 40.0	Pál et al. (2008)	1.5 ± 0.2	Bonfanti et al. (2015)
HD 188015	7.93 ± 0.04	Ofek (2008)	57.0 ± 2.9	van Leeuwen (2007)	$5.3^{+2.6}_{-0.3}$	Ramírez et al. (2012)
HD 190360	5.41 ± 0.04	Ofek (2008)	15.9 ± 0.1	van Leeuwen (2007)	$11.5^{+1.3}_{-2.8}$	Ramírez et al. (2012)
HD 197037	6.63 ± 0.03	Ofek (2008)	32.3 ± 0.4	van Leeuwen (2007)	0.3 ± 0.3	Bonfanti et al. (2015)
HD 206610	7.87 ± 0.04	Ofek (2008)	193.8 ± 43.7	van Leeuwen (2007)	2.1 ± 0.3	Bonfanti et al. (2015)
HD 208527	4.78 ± 0.13	Ofek (2008)	403.2 ± 73.0	van Leeuwen (2007)	2.0 ± 1.3	Lee, Han & Park (2013)
HD 210277	6.23 ± 0.04	Ofek (2008)	21.6 ± 0.2	van Leeuwen (2007)	7.9 ± 2.0	Bonfanti et al. (2015)
HD 217786	7.54 ± 0.02	Ofek (2008)	54.9 ± 2.3	van Leeuwen (2007)	6.5 ± 0.8	Bonfanti et al. (2015)
HD 240210	7.16 ± 0.13	Jester et al. (2005)	143.0 ± 53.0	Niedzielski et al. (2009)	10.9 ± 1.8	Bonfanti et al. (2015)
HD 219828	7.78 ± 0.03	Ofek (2008)	72.3 ± 4.1	van Leeuwen (2007)	5.0 ± 0.7	Bonfanti et al. (2015)
HD 220074	4.77 ± 0.07	Ofek (2008)	324.7 ± 52.7	van Leeuwen (2007)	4.5 ± 2.8	Lee et al. (2013)
HD 222155	6.86 ± 0.02	Ofek (2008)	49.1 ± 1.5	van Leeuwen (2007)	7.9 ± 0.1	Bonfanti et al. (2015)

Table 6. Absolute magnitude and derived masses for all confirmed or possible companions detected in our survey. The absolute magnitude refers to the SDSS *i* band. If multiple measurements were available, we give the average absolute magnitude.

Object	Abs. mag. (mag)	Mass ($M_\odot$)
HD 2638	8.63 ± 0.45	$0.425^{+0.067}_{-0.095}$
HAT-P-7	10.40 ± 0.28	$0.205^{+0.026}_{-0.021}$
HD 185269[a]	10.10 ± 0.13	$0.232^{+0.012}_{-0.012}$
WASP-76	6.50 ± 0.45	$0.692^{+0.074}_{-0.059}$
HAT-P-32	9.00 ± 0.15	$0.340^{+0.048}_{-0.024}$
HD 10697	10.75 ± 0.18	$0.177^{+0.013}_{-0.010}$
HD 43691[a]	11.06 ± 0.19	$0.160^{+0.010}_{-0.010}$
HD 116029	10.7 ± 1.8	$0.18^{+0.21}_{-0.07}$
HAT-P-18	13.21 ± 0.17	$0.0994^{+0.0022}_{-0.0016}$
Kepler-21	$8.6^{+4.2}_{-1.0}$	$0.42^{+0.14}_{-0.32}$
Kepler-68	10.78 ± 0.18	$0.175^{+0.013}_{-0.010}$
Kepler-42	15.59 ± 0.62	$0.0819^{+0.0035}_{-0.0029}$
HD 197037	9.225 ± 0.066	$0.3412^{+0.0098}_{-0.0477}$
HD 217786	11.02 ± 0.13	$0.1622^{+0.0071}_{-0.0068}$

Note. [a]we give the unresolved magnitude and the derived mass from that unresolved magnitude.

Table 7. SPHERE photometric measurements and mass estimates of the resolved components of the binary HD 185269 B. The primary star is saturated in *Y* and *H* band, and thus masses and differential magnitudes could only be calculated in *J* band.

Filter	BB_Y	BB_J	BB_H
ΔBa/Bb [mag]	0.24 ± 0.11	0.14 ± 0.12	0.21 ± 0.04
ΔA/Ba [mag]	–	6.957 ± 0.082	–
ΔA/Bb [mag]	–	7.093 ± 0.088	–
mass Ba [$M_\odot$]	–	0.165 ± 0.08	–
mass Bb [$M_\odot$]	–	$0.154^{+0.009}_{-0.008}$	–

components. As mentioned previously the primary star is saturated in *Y* and *H* band, thus in these bands we could only measure the brightness difference between the binary components. However, our *J*-band data are unsaturated, which enabled photometric calibration of the binary measurements with the primary star. We list all our results in Table 7. The given *J*-band magnitudes are assuming that the neutral density filter is flat across the covered wavelength range.

We used again the BT-SETTL models to convert the *J*-band measurements into masses of the individual components. For this conversion, we utilized the *J*-band magnitude of the primary of 5.518 ± 0.027 mag (Cutri et al. 2003) and the most recent age estimate by Pace (2013) of 3.49 ± 0.79 Gyr. The system is located at a distance of 47.37 ± 1.72 pc (van Leeuwen 2007). Given the brightness of the binary components, we calculate masses of 0.165 ± 0.008 $M_\odot$ and $0.154^{+0.009}_{-0.008}$ $M_\odot$ for the Ba and Bb components, respectively.

To compare these results with our unresolved SDSS *i*-band measurements, we calculated the flux ratio between the two components in *Y* band. Given the differential brightness measured in our SPHERE image, the flux ratio between the two components is 0.8. To verify that this flux ratio is consistent with our AstraLux observations in SDSS *i* band, we used the results obtained from PSF fitting of the two components of HD 185269 B in the 2013 AstraLux data mentioned in Section 3. This PSF fitting yields a flux ratio of 0.78, i.e. consistent with the *Y*-band results obtained with SPHERE. We calculated the expected apparent SDSS *i*-band magnitudes for both components to be 14.12 ± 0.10 and 14.36 ± 0.10 mag. From these measurements we derived SDSS *i*-band masses of 0.18 ± 0.01 and 0.16 ± 0.01 $M_\odot$ for the Ba and Bb component, respectively. These are consistent with our more precise *J*-band masses within 1σ.

4.4 WASP-76

For WASP-76, we find a differential magnitude in the SDSS *i* band of 2.58 ± 0.27 mag. This is very consistent with the value of 2.51 ± 0.25 mag recovered by Wöllert & Brandner (2015), using the same instrument setup. Given our differential magnitude and the age, distance and apparent magnitude of the primary star shown in Table 5, we compute a mass of the object of $0.692^{+0.074}_{-0.059}$ $M_\odot$, assuming that it is indeed gravitationally bound.

4.5 HAT-P-32

In the case of the HAT-P-32 system, we find a differential SDSS *i*-band magnitude of 5.403 ± 0.057 mag for the stellar companion. Given the age, distance and apparent magnitude of the primary star this translates into a mass of $0.340^{+0.048}_{-0.024}$ $M_\odot$. The mass of HAT-P-32 B was also recently estimated by Ngo et al. (2015), who detected the companion in *J*, *H* and *K* band. They arrived at a mass of 0.393 ± 0.012 $M_\odot$ for *J* and *K* band, and 0.4243 ± 0.0085 $M_\odot$ for *H* band. Our mass estimate is lower but marginally consistent within 1σ with their *J* and *K* band results. We are deviating from their higher *H*-band mass by 1.5 σ. However, we want to point out that their two mass estimates also deviate by a similar margin. In principle, it is possible that our slightly lower mass estimate is caused by an overestimation of the background, which is dominated by the bright stellar halo, even though we get consistent photometric results with other studies for sources at even smaller separations, such as WASP-76.

5 DETECTION LIMITS

To guide future observations and enable more sophisticated statistical analysis of the multiplicity ratio of exoplanet hosts, we have derived detection limits at various separations for each of our target stars. For this purpose, we first computed the achievable magnitude difference (contrast) compared to the bright primary star at these separations. We assume that an object is detectable when its signal-to-noise ratio is equal or larger than 5. We then use the peak brightness of the bright primary star as calibration value for the signal. The noise at each separation is determined by averaging over the standard deviation measured in 5×5 pixel boxes which are centred on each pixel with the respective separation from the primary star. In Fig. 6, we show the average contrast of all our observations along with the best and worst contrast achieved up to a separation of 5 arcsec, at which we reach the background limit. To convert from these magnitude limits to mass limits, we again utilized the BT-SETTL models as described in Section 4. The input values for this conversion are given in Table 5. The final derived mass limits are given in Table 8. In some cases not all necessary input values were available; we then give only the achievable magnitude limit, which can be used to calculate mass limits at a later time, should all the input values become available. In addition, in a few cases the detectable minimum mass was located outside of our model grid. We then give a lower or upper detection limit based on the closest grid value.

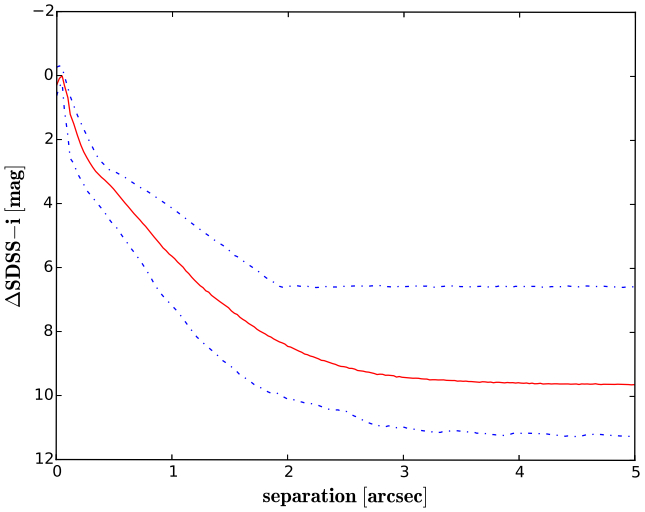

Figure 6. Contrast achieved in our AstraLux observations. We show the average contrast (solid, red line) as well as the best and worst contrast (dash–dotted, blue lines). The contrast depends strongly on the observing conditions, which explains the large spread between the best and worst contrast. Individual contrast curves for each target are available as supplementary online material.

Our detection limits depend mostly on the atmospheric conditions during the observations as well as the brightness and distance of the exoplanet host. Since our sample consists mostly of evolved systems with typical ages in the order of a few Gyr, the dependence of the detectable mass limit on the age is less important. We are on average sensitive to masses down to 0.52 $M_{\odot}$ outside of 1 arcsec and down to 0.16 $M_{\odot}$ in the background limited region outside of 5 arcsec. These detection limits are comparable to our previous study Ginski et al. (2012) in which we used AstraLux on a similar sample of target systems.

6 DISCUSSION OF THE NEW BOUND STELLAR COMPANIONS

6.1 Kepler-21

Kepler-21 (also known as HD 179070, KOI-975, KIC 3632418) is the brightest star in the original *Kepler* sample. Howell et al. (2012) found a transiting planet of approximately 1.6 times the size of the earth in an ∼2.8 d orbit around this star. According to them, the planet has an upper mass limit of 10.5 Earth masses and is moving on a circular orbit. They also carried out high-resolution adaptive optics imaging of the host star with the Keck telescope in the near-infrared. In these images taken on 2011-02-22 they detected a faint source with a separation of 0.75 arcsec at a PA of 129 deg. This source is identical to the source that we detected with AstraLux in our 2013 and 2014 observations and that emerged as new comoving low-mass stellar companion. We introduce this companion here as a new discovery, because Howell et al. (2012) exclude the possibility that the source is physically associated with the host star based on its J–K_s colour. They argue that the colour of the companion is either consistent with a late M dwarf which should then be located at ∼15 pc or with a M0 giant, which would be located in an approximate distance of 10 kpc. Since Kepler-21 is located at approximately 112 pc, the two sources should then not be associated. However, our own astrometric measurements in 2013 and 2014 show clearly that the source is comoving with Kepler-21. In fact, also the astrometric position given by Howell et al. (2012) in their 2011 Keck measurement is perfectly consistent with a comoving object. If the object was indeed a background giant in some kpc distance, we would have expected a PA of 119.6 deg at the time of the 2011 measurement. Unfortunately Howell et al. (2012) do not provide uncertainties for their astrometric measurements. However, a deviation of almost 10 deg seems very unlikely. To get an estimate of the likelihood to detect a background or foreground object within 0.77 arcsec around Kepler-21 we followed the approach by Lillo-Box et al. (2014). They give the probability to find a physically unrelated source within a certain distance of a star with

$$P(r, b, m_{\odot}, \Delta m_{\max}) = \pi r^2 \rho(b, m_{\odot}, \Delta m_{\max}), \quad (1)$$

wherein r is the separation from the star, b is the galactic latitude, $m_{\odot}$ is the apparent magnitude of the star in the observed filter, $\Delta m_{\max}$ is the maximum achieved contrast within the separation r, and ρ is the stellar density. To estimate the stellar density as a function of the galactic latitude and the achieved magnitude limit, we utilize the TRILEGAL[4] population synthesis code by Girardi et al. (2005). We choose the default parameters for the different parts of the Galaxy and the lognormal initial mass function of Chabrier (2001). We find that in an area of 1 deg^2 around Kepler-21 we should be able to detect 452 stars with a limiting magnitude of 12.86 mag in SDSS i band. The limiting magnitude is the value that we are computing as described in Section 5 for a separation of 0.8 arcsec. This yields a stellar density ρ of 3.5×10^{-5} sources per arcsec^2. Putting this into equation (1) we find a probability of 6.5×10^{-5} to detect an unrelated background or foreground source within 0.77 arcsec of Kepler-21. We thus conclude that, given our astrometry, the most likely explanation is indeed that the companion candidate is physically bound to Kepler-21.

Kepler-21 B is located at a projected separation of only 87 au, which might indicate that it should have had a strong influence on the planet formation process. One possible scenario might be that the stellar companion excited high eccentricities in the forming planet causing close encounters with the primary star. The eccentricity could have then been damped by tidal heating which would have left the companion on a very short periodic circular orbit. Such scenarios have been suggested to occur in multiple planetary systems, where multiple objects interact dynamically, e.g. by Rasio & Ford (1996). Given that the system is evolved (∼3.6 Gyr), it is consistent that we would now observe the end product of this interaction.

6.2 Kepler-68

The star Kepler-68 hosts three known planets detected via transit and radial velocity observations by Gilliland et al. (2013). The innermost two of these planets have orbit periods in the order of days and masses in the order of several Earth masses and were detected in transit, while the outer planet d was found in radial velocity data and has a much longer orbit period of ∼1.6 yr (semimajor axis of 1.4 au) and higher mass ($m \cdot \sin(i) = 0.95$ $M_{\rm Jup}$). The inner planets appear to be on circular orbits, while the outer planet exhibits an orbit eccentricity of 0.18.

The newly discovered stellar component Kepler-68 B is located at a projected separation of 1485 au. Due to this large separation, the expected period of Kozai–Lidov type resonances is in the order of several Gyr. It seems thus unlikely that the stellar component has a major influence on the dynamics of the inner system via this

[4] http://stev.oapd.inaf.it/cgi-bin/trilegal_1.6

Table 8. Detection limits of all stars observed in our survey. We give the achievable magnitude difference as well as the corresponding mass limit.

	0.5 arcsec		1 arcsec		2.5 arcsec		5 arcsec	
Star	Δ mag	$M_{\rm min}$ ($M_\odot$)	Δ mag	$M_{\rm min}$ ($M_\odot$)	Δ mag	$M_{\rm min}$ ($M_\odot$)	Δ mag	$M_{\rm min}$ ($M_\odot$)
HD 2638	3.3	$0.402^{+0.062}_{-0.091}$	5.3	$0.171^{+0.028}_{-0.059}$	9.0	$0.0878^{+0.0028}_{-0.043}$	9.6	$0.0843^{+0.0027}_{-0.045}$
HD 2952	3.8	–	6.4	–	10.3	–	10.9	–
HD 5608	2.8	–	4.1	–	7.7	–	9.9	–
HD 5891	2.9	$1.22^{+0.18}_{-1.20}$	4.0	$1.00^{+0.18}_{-0.15}$	7.5	$0.52^{+0.12}_{-0.13}$	9.5	$0.243^{+0.12}_{-0.076}$
HD 8574	3.9	$0.5564^{+0.0068}_{-0.0060}$	6.9	$0.1868^{+0.0039}_{-0.0034}$	10.4	$0.090\,28^{+0.000\,54}_{-0.000\,43}$	10.8	$0.088\,00^{+0.000\,34}_{-0.000\,28}$
HD 10697	3.8	$0.614^{+0.019}_{-0.019}$	6.3	$0.275^{+0.019}_{-0.019}$	9.9	$0.0994^{+0.0021}_{-0.0015}$	10.1	$0.0974^{+0.0017}_{-0.0016}$
WASP-76	3.3	$0.60^{+0.11}_{-0.11}$	5.3	$0.34^{+0.13}_{-0.14}$	8.7	$0.108^{+0.022}_{-0.049}$	9.1	$0.102^{+0.016}_{-0.047}$
HAT-P-32	3.9	$0.554^{+0.054}_{-0.028}$	6.0	$0.253^{+0.063}_{-0.030}$	8.4	$0.0871^{+0.024}_{-0.0074}$	8.5	$0.0826^{+0.027}_{-0.0071}$
HD 12661	3.7	$0.498^{+0.015}_{-0.017}$	6.1	$0.198\,23^{+0.010}_{-0.0083}$	9.8	$0.0901^{+0.0013}_{-0.0011}$	10.0	$0.0881^{+0.0011}_{-0.0014}$
HD 13189	3.7	–	5.7	–	9.9	–	10.3	–
HD 13908	3.8	$0.655^{+0.034}_{-0.032}$	6.2	$0.329^{+0.039}_{-0.037}$	9.8	$0.1046^{+0.0037}_{-0.0036}$	10.1	$0.0997^{+0.0036}_{-0.0026}$
HD 15779	2.9	–	3.9	–	7.4	–	9.8	–
HD 285507	3.8	$0.189^{+0.019}_{-0.016}$	5.0	$0.1266^{+0.0085}_{-0.0069}$	8.6	$0.0762^{+0.0029}_{-0.0032}$	9.0	$0.0726^{+0.0029}_{-0.0035}$
HD 290327	3.3	$0.480^{+0.062}_{-0.070}$	4.5	$0.301^{+0.076}_{-0.056}$	8.0	$0.1041^{+0.0080}_{-0.0060}$	8.6	$0.0965^{+0.0054}_{-0.0048}$
HD 40979	3.4	$0.5946^{+0.0095}_{-0.0095}$	5.2	$0.347^{+0.011}_{-0.011}$	9.0	$0.1025^{+0.0011}_{-0.0010}$	9.8	$0.093\,99^{+0.000\,97}_{-0.000\,74}$
HD 43691	3.5	$0.652^{+0.051}_{-0.047}$	4.9	$0.477^{+0.051}_{-0.054}$	7.7	$0.160^{+0.021}_{-0.017}$	8.3	$0.133^{+0.014}_{-0.011}$
HD 45350	3.5	$0.562^{+0.023}_{-0.023}$	5.1	$0.337^{+0.029}_{-0.027}$	8.7	$0.1054^{+0.0026}_{-0.0025}$	9.7	$0.0942^{+0.0019}_{-0.0017}$
Omi Uma	3.5	>1.4	5.2	$1.017^{+0.013}_{-0.011}$	8.9	$0.4966^{+0.0080}_{-0.0076}$	9.6	$0.3937^{+0.0091}_{-0.0084}$
GJ328	3.3	–	4.4	–	7.5	–	8.2	–
HD 95089	3.3	$0.914^{+0.11}_{-0.098}$	5.0	$0.671^{+0.082}_{-0.080}$	8.6	$0.212^{+0.067}_{-0.046}$	9.5	$0.155^{+0.040}_{-0.027}$
HD 96063	3.1	$0.91^{+0.13}_{-0.11}$	4.2	$0.756^{+0.11}_{-0.092}$	7.9	$0.282^{+0.11}_{-0.075}$	9.2	$0.166^{+0.056}_{-0.034}$
HD 99706	3.5	$0.887^{+0.077}_{-0.070}$	5.3	$0.652^{+0.060}_{-0.059}$	8.7	$0.213^{+0.047}_{-0.037}$	9.3	$0.170^{+0.034}_{-0.024}$
HD 100655	3.3	$1.150^{+0.084}_{-0.072}$	4.9	$0.848^{+0.055}_{-0.050}$	8.9	$0.320^{+0.050}_{-0.045}$	9.7	$0.225^{+0.035}_{-0.030}$
HIP 57274	3.4	$0.285^{+0.021}_{-0.017}$	4.6	$0.1740^{+0.0099}_{-0.0076}$	7.4	$0.0958^{+0.0014}_{-0.0013}$	7.7	$0.0931^{+0.0014}_{-0.0014}$
HD 102329	3.3	$0.97^{+0.14}_{-0.12}$	4.8	$0.745^{+0.11}_{-0.094}$	8.5	$0.263^{+0.10}_{-0.071}$	9.8	$0.156^{+0.050}_{-0.030}$
HD 106270	3.1	$0.806^{+0.051}_{-0.047}$	4.4	$0.643^{+0.045}_{-0.043}$	7.8	$0.203^{+0.033}_{-0.026}$	8.8	$0.145^{+0.018}_{-0.014}$
HD 113337	3.6	$0.671^{+0.012}_{-0.013}$	5.6	$0.405^{+0.022}_{-0.021}$	9.3	$0.0819^{+0.015}_{-0.0076}$	9.6	$0.0752^{+0.019}_{-0.0066}$
HD 116029	4.1	$0.751^{+0.060}_{-0.054}$	7.1	$0.372^{+0.066}_{-0.064}$	10.2	$0.120^{+0.014}_{-0.011}$	10.3	$0.1155^{+0.013}_{-0.0089}$
HD 120084	3.4	$1.148^{+0.035}_{-0.030}$	4.8	$0.896^{+0.024}_{-0.021}$	8.8	$0.356^{+0.020}_{-0.019}$	9.8	$0.227^{+0.013}_{-0.012}$
Beta UMi	3.5	>1.3	4.6	>1.3	8.0	$0.7522^{+0.010}_{-0.0084}$	9.6	$0.5536^{+0.0073}_{-0.0064}$
HD 131496	4.0	$0.741^{+0.062}_{-0.057}$	6.9	$0.370^{+0.071}_{-0.069}$	10.1	$0.117^{+0.014}_{-0.010}$	10.3	$0.1115^{+0.014}_{-0.0072}$
HD 136726	4.2	$1.240^{+0.071}_{-0.045}$	7.0	$0.777^{+0.021}_{-0.020}$	10.3	$0.349^{+0.021}_{-0.020}$	10.5	$0.320^{+0.022}_{-0.020}$
HD 136512	4.1	$0.953^{+0.056}_{-0.046}$	7.0	$0.583^{+0.027}_{-0.026}$	10.5	$0.170^{+0.013}_{-0.011}$	10.7	$0.160^{+0.011}_{-0.011}$
HD 139357	4.4	$1.03^{+0.19}_{-1.00}$	7.3	$0.674^{+0.068}_{-0.065}$	10.2	$0.291^{+0.079}_{-0.058}$	10.3	$0.283^{+0.076}_{-0.056}$
HD 145457	4.5	$0.896^{+0.053}_{-0.049}$	7.2	$0.536^{+0.040}_{-0.041}$	10.3	$0.170^{+0.021}_{-0.017}$	10.4	$0.163^{+0.019}_{-0.016}$
HD 152581	3.9	$0.79^{+0.15}_{-0.13}$	6.8	$0.46^{+0.14}_{-0.16}$	9.7	$0.146^{+0.069}_{-0.036}$	9.8	$0.142^{+0.064}_{-0.033}$
HAT-P-18	4.1	$0.222^{+0.028}_{-0.023}$	6.6	$0.1067^{+0.0045}_{-0.0037}$	7.9	$0.0923^{+0.0028}_{-0.0025}$	8.0	$0.0915^{+0.0028}_{-0.0021}$
HD 156279	4.0	$0.389^{+0.015}_{-0.013}$	6.5	$0.1478^{+0.0039}_{-0.0035}$	10.0	$0.085\,98^{+0.000\,50}_{-0.000\,50}$	10.3	$0.084\,71^{+0.000\,50}_{-0.000\,50}$
HD 163607	3.7	$0.609^{+0.020}_{-0.018}$	6.2	$0.271^{+0.019}_{-0.018}$	9.6	$0.1019^{+0.0023}_{-0.0022}$	9.8	$0.0991^{+0.0020}_{-0.0015}$
HD 163917	3.8	$1.289^{+0.021}_{-0.019}$	6.6	$0.7652^{+0.0095}_{-0.0095}$	10.5	$0.2481^{+0.0075}_{-0.0072}$	11.2	$0.1843^{+0.0050}_{-0.0048}$
HIP 91258	3.4	$0.451^{+0.024}_{-0.044}$	5.0	$0.234^{+0.016}_{-0.055}$	8.7	$0.0939^{+0.0016}_{-0.040}$	9.8	$0.085\,82^{+0.000\,99}_{-0.042}$
Kepler-37	3.5	$0.40^{+0.33}_{-0.25}$	5.5	$0.177^{+0.30}_{-0.078}$	9.0	$0.089^{+0.040}_{-0.013}$	9.5	$0.086^{+0.027}_{-0.011}$
Kepler-21	3.7	$0.691^{+0.043}_{-0.043}$	6.0	$0.395^{+0.052}_{-0.051}$	9.0	$0.129^{+0.014}_{-0.010}$	9.2	$0.124^{+0.012}_{-0.010}$
HD 180314	4.4	$0.924^{+0.054}_{-0.048}$	7.2	$0.544^{+0.035}_{-0.035}$	10.2	$0.176^{+0.020}_{-0.019}$	10.4	$0.168^{+0.018}_{-0.017}$
Kepler-63	3.7	$0.424^{+0.059}_{-0.063}$	5.8	$0.171^{+0.034}_{-0.032}$	8.0	$0.081^{+0.014}_{-0.011}$	8.1	$0.081^{+0.014}_{-0.012}$
Kepler-68	4.0	$0.485^{+0.049}_{-0.054}$	6.6	$0.175^{+0.027}_{-0.020}$	9.0	$0.1003^{+0.0052}_{-0.0038}$	9.1	$0.0985^{+0.0046}_{-0.0037}$
Kepler-42	4.8	$0.0794^{+0.0045}_{-0.0040}$	6.4	$0.0760^{+0.0020}_{-0.0061}$	6.6	$0.0756^{+0.0020}_{-0.0062}$	6.6	$0.0757^{+0.0020}_{-0.0062}$
HAT-P-7	3.6	$0.704^{+0.082}_{-0.079}$	5.9	$0.414^{+0.090}_{-0.090}$	8.8	$0.136^{+0.029}_{-0.019}$	9.0	$0.127^{+0.025}_{-0.018}$

Table 8 – *continued*

Star	0.5 arcsec		1 arcsec		2.5 arcsec		5 arcsec	
	Δ mag	$M_{\rm min}$ ($M_\odot$)	Δ mag	$M_{\rm min}$ ($M_\odot$)	Δ mag	$M_{\rm min}$ ($M_\odot$)	Δ mag	$M_{\rm min}$ ($M_\odot$)
HD 188015	4.5	$0.424^{+0.040}_{-0.040}$	7.3	$0.143^{+0.012}_{-0.010}$	10.3	$0.0881^{+0.0015}_{-0.0015}$	10.5	$0.0870^{+0.0015}_{-0.0015}$
HD 190360	3.7	$0.4873^{+0.0088}_{-0.0062}$	6.2	$0.1886^{+0.0042}_{-0.0031}$	9.9	$0.089\,02^{+0.000\,31}_{-0.000\,28}$	10.3	$0.087\,10^{+0.000\,31}_{-0.000\,25}$
HD 197037	3.8	$0.5255^{+0.0087}_{-0.024}$	6.2	$0.212^{+0.011}_{-0.043}$	10.0	$0.077^{+0.011}_{-0.025}$	10.4	$0.072^{+0.012}_{-0.024}$
HD 206610	3.2	$0.97^{+0.21}_{-0.17}$	4.8	$0.74^{+0.16}_{-0.14}$	8.6	$0.240^{+0.15}_{-0.084}$	9.6	$0.161^{+0.088}_{-0.043}$
HD 208527	4.0	>1.4	6.9	$1.16^{+0.24}_{-1.2}$	10.1	$0.66^{+0.12}_{-0.11}$	10.3	$0.63^{+0.12}_{-0.11}$
HD 210277	3.3	$0.5234^{+0.0099}_{-0.0089}$	5.7	$0.2152^{+0.0070}_{-0.0064}$	9.6	$0.090\,15^{+0.000\,69}_{-0.000\,42}$	10.2	$0.086\,45^{+0.000\,40}_{-0.000\,36}$
HD 217786	4.0	$0.532^{+0.027}_{-0.025}$	5.4	$0.322^{+0.031}_{-0.029}$	9.5	$0.0984^{+0.0023}_{-0.0020}$	9.8	$0.0948^{+0.0020}_{-0.0020}$
HD 240210	3.6	$0.85^{+0.35}_{-0.85}$	5.8	$0.61^{+0.22}_{-0.25}$	9.7	$0.159^{+0.17}_{-0.056}$	10.4	$0.129^{+0.12}_{-0.034}$
HD 219828	4.1	$0.559^{+0.035}_{-0.035}$	7.0	$0.194^{+0.024}_{-0.020}$	9.8	$0.0984^{+0.0033}_{-0.0028}$	9.9	$0.0974^{+0.0029}_{-0.0027}$
HD 220074	3.7	>1.2	6.1	$1.16^{+0.24}_{-1.2}$	9.8	$0.64^{+0.11}_{-0.10}$	10.2	$0.58^{+0.11}_{-0.10}$
HD 222155	3.4	$0.654^{+0.019}_{-0.019}$	4.9	$0.468^{+0.023}_{-0.021}$	8.8	$0.1177^{+0.0045}_{-0.0043}$	9.6	$0.1026^{+0.0023}_{-0.0021}$

mechanism. It remains unclear if such a widely separated outer stellar component has a strong influence on the circumstellar disc in the planet formation phase. Following the argument of Kraus et al. (2012), who studied the occurrence rate of circumstellar discs in young binary systems, a major influence of the secondary stellar component is only expected for separations of up to 40 au. If this observational result holds true, then Kepler-68 B is too widely separated to have influenced the circumstellar disc around Kepler-68 A. However, it is in principle also possible that the B component is on a very eccentric orbit. If this is the case then close interactions with the inner planets or the planet forming disc might have happened. In the case of a very eccentric orbit, we would expect to find the stellar companion at a wide separation since it spends the majority of the time there. Further high precision astrometric monitoring combined with statistical orbit analysis might shed some light on the orbit of the B component.

Since the source that we now identified as Kepler-68 B was detected in 2MASS, it was included in the Kepler input catalogue. With its large separation of 11 arcsec the new stellar component is not within the 'classical' Kepler PSF. However, Kepler-68 is strongly saturated and shows bleeding. Therefore, the changes in flux can only be seen at the end of bleed columns. Gilliland et al. (2013) showed that Kepler-68 B is located almost precisely in the column direction from Kepler-68. In most of the observing quarters of *Kepler*, the bleeding encompasses Kepler-68 B and, hence, has to be taken into account for the transit measurements. If the light contribution of B is not considered, systematic errors in the system parameters will arise without changing the quality of the transit fit. From the measured magnitude difference of 6.6 mag (see Table 3), we calculated the amount of contaminating light. If B is a binary that exhibits total eclipses, the transit depth measured by *Kepler* would be 2300 ppm. This is much higher than the detected transit depth of 346 ppm and 55 ppm for Kepler-68 b and Kepler-68 c, respectively (Gilliland et al. 2013). Therefore a partial or grazing eclipse of B could produce a transit signal. However, as shown before by e.g. Latham et al. (2011) or Fressin et al. (2011), it is very unlikely that an eclipsing background object can mimic a multiple planetary system. Furthermore Gilliland et al. (2013) showed that in Quarter 9 Kepler-68 as well as Kepler-68 B are located between columns in such a way that the bleeding terminates before reaching the latter. In this way they proved that Kepler-68 B cannot be the source of the transit signal. Finally, by applying the BLENDER procedure (Torres et al. 2004; Fressin et al. 2011), Gilliland et al. (2013) could rule out all false positive scenarios involving eclipsing binaries and validate Kapler-68 b,c as planets.

6.3 HD 197037

HD 197037 hosts an $m{\cdot}\sin(i) = 0.79$ $M_{\rm Jup}$ planet on an ∼2.8 yr period (semimajor axis of 2.1 au), discovered by Robertson et al. (2012). They found that their best-fitting orbit solution for the planet exhibits an eccentricity of 0.22. They also note that they include in their model a linear trend in radial velocity with a slope of -1.87 ± 0.3 $ms^{-1}yr^{-1}$, which could be attributed to a long period planet of 0.7 $M_{\rm Jup}$ and a period of ∼12 yr, or possibly a more distant stellar companion of which they find no further evidence.

To determine if the newly detected stellar companion HD 197037 B can be responsible for this linear trend in the radial velocity, we performed a dedicated Monte Carlo simulation. We fixed the system mass to the combined mass of both stellar components, i.e. 0.34 $M_\odot$ for B and 1.11 $M_\odot$ for A (Robertson et al. 2012). We then generated random bound Keplerian orbits which are compatible with our astrometric measurement of HD 197037 B. To somewhat narrow the wide parameter space, we restricted our simulation to orbits with a semimajor axis between 3 and 6 arcsec and times of periastron passage within 2000 yr from our astrometric epoch. We created a total of 15 000 such orbits. We then checked which of these orbits would introduce a slope as measured by Robertson et al. (2012) in their measurement period between the beginning of 2001 and 2012. Out of the 15 000 randomly generated orbits, 1217 orbits fulfill this criterion. In Fig. 7, we show the eccentricities and orbit inclinations of all these orbits. We find that there is no strongly preferred region of the parameter space for an orbit of the B component to produce the measured radial velocity slope. In particular we find orbits for the full range of possible eccentricities. The range of possible inclinations is constrained only by the photometric mass estimate of the B component, i.e. the orbit needs to have a minimum inclination of ∼18 deg to produce the radial velocity signal. From our imaging epochs we cannot yet constrain the orbit of the B component, i.e. it is in principle possible that the B component is in a face-on or close to face-on orbit configuration. However given the large range of orbit solutions of the B component that reproduce the measured linear radial velocity trend, we find it

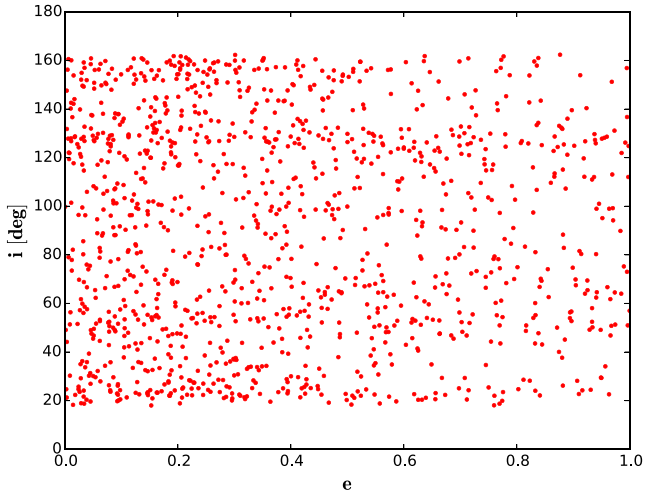

Figure 7. Inclination and eccentricity distribution for possible orbits of HD 197037 B that induce a linear trend in the radial velocity of HD 197037 A as measured by Robertson et al. (2012). Shown are 1217 out of 15 000 randomly generated bound Keplerian orbits that include the current position of HD 197037 B and that match the total system mass.

likely that this trend is indeed caused by the stellar B component and not by an additional long period planet.

The non-circular orbit of the existing extrasolar planet around the A component might also be well explained by the new stellar companion if they are caught in mutual Kozai–Lidov type resonances. Given the potential very young age of the system of 0.3±0.3 Gyr (Bonfanti et al. 2015), it may also be possible that the stellar B component was not originally a part of the system but was just caught as the result of a stellar flyby in more recent times. This would then have disrupted the original circular orbit of the planet. However, since HD 197037 is not a known member of a star-forming region or young moving group, such an event would seem rather unlikely.

6.4 HD 217786

Moutou et al. (2011) discovered a long period (∼3.6 yr) planet or brown dwarf with a minimum mass of 13 M_{Jup} around HD 217786 via radial velocity measurements. They found that the best-fitting orbit solution of the object is very eccentric with $e = 0.4 \pm 0.05$. They do not see long-term radial velocity trends in their data.

The new stellar companion HD 217786 B is located at a projected separation of 155 au. To explore whether the large eccentricity of the planetary companion could be caused by Kozai–Lidov resonances with the stellar companion, we calculated the period of possible Kozai cycles. For this purpose we used the formula provided in Takeda & Rasio (2005). We assumed that the semimajor axis of the orbit of the stellar companion is equal to its projected separation and that the orbit is circular. We get a period of ∼6.2 Myr. This period can be approximately an order of magnitude shorter if the stellar companion is on a significantly eccentric orbit itself. Given the large system age of ∼6.5 Gyr, more than a thousand Kozai cycles could have been complete in principle. It is thus conceivable that the eccentricity of the planetary companion is indeed caused by such interactions with the newly discovered stellar companion. However, this is just one possible scenario to explain the eccentricity of the planet and it strongly depends on the actual orbit of the new stellar companion.

7 SUMMARY

We searched for stellar companions around 60 stars known to harbour extrasolar planets using AstraLux at the Calar Alto observatory. We found previously unknown faint companion candidates within the field of view of our observations around 11 of the observed systems. Of these companion candidates, four, namely Kepler-21 B, Kepler-68 B, HD 197037 B and HD 217786 B, emerged as comoving, and thus in all likelihood gravitationally bound, companions. The candidates detected around HD 188015 and Kepler-37 are more consistent with background objects. For the remaining five systems follow-up lucky imaging observations must still be performed to determine the status of the objects, i.e. if they are comoving with the exoplanet host star. The candidate found next to HD 43691 might be of special interest since it may be a low-mass binary itself.

We also present new photometric and astrometric measurements for the previously known companions to the HD 2638, HAT-P-7, HD 185269, WASP-76 and HAT-P-32 systems. Our SPHERE observations of HD 185269 B showed that the companion is actually a very low mass binary itself, making the system one of only 17 triple systems known to harbour extrasolar planets. Continued astrometric monitoring within the next decade will allow us to determine the dynamical mass of the binary companion.

We note that the previously detected companion candidate to WASP-76 (Wöllert & Brandner 2015) is more consistent with a background source given our new astrometric measurement; however, no final conclusion could be drawn due to the short time baseline between the two observational epochs.

Including the first part of our survey presented in Ginski et al. (2012), we have now studied the multiplicity of 125 known exoplanet systems. In this sample we found so far seven new confirmed binary systems. This includes the new systems reported by us in this work and in Ginski et al. (2012), as well as all systems that were first reported in other studies, but that were unknown at the time of our first epoch observation. This yields a multiplicity rate of only 5.6 per cent in our sample. This is much lower than previous values reported by (Roell et al. 2012, 12 per cent), (Mugrauer et al. 2014, 13 per cent) or (Mugrauer & Ginski 2015, 9 per cent). If most of the unconfirmed companions that we report in this study turn out to be bound companions, the multiplicity rate of our study would increase to 9–10 per cent, which would be in better agreement with previous results. One contributing factor to our lower multiplicity rate might be that the majority of our sample is comprised of planetary systems found via the radial velocity method. Radial velocity surveys routinely exclude known binary systems from their target sample. Thus they introduce an inherent bias towards single star systems. However, the same was in principle true for the studies by Mugrauer et al. (2014) and Mugrauer & Ginski (2015).

If the low multiplicity rate that we recover is indeed caused by a bias introduced by radial velocity surveys, then it would be expected that a higher stellar multiplicity rate is found for transiting planets. Wang et al. (2015) present the results of an adaptive optics imaging search around 138 Kepler planet hosts. They find a stellar multiplicity rate of 8.0 ± 4.0 per cent for multiplanet systems and 6.4 ± 5.8 per cent for single-planet systems and stellar companions with semimajor axes between 100 and 2000 au. These values are in principle consistent with the stellar multiplicity rate of 5.6 per cent that we find, which might indicate that the selection bias of radial velocity surveys has no significant influence on our result. However, from a statistical point of view, considering simple random sampling, our sample size is too small for accurate predictions. If we assume a confidence level of 95 per cent, then our estimated

level of accuracy for a population size of 1200 exoplanet systems is only 8.2 per cent. Given that our sample is definitely biased towards single star systems, our actual level of accuracy will be worse than this estimate. To get a reliable estimate of the stellar multiplicity of exoplanet systems with a margin of error on the 5 per cent level, a random sample size of 291 systems is necessary considering the known population of ∼1200 confirmed systems. If we consider a much larger population, i.e. all planetary systems in the Galaxy, then a larger random sample size of 385 systems is needed. These are again lower limits considering the potential biases introduced by exoplanet surveys. We are continuing our multiplicity survey in order to provide a homogeneous observation base for statistical analysis.

ACKNOWLEDGEMENTS

We would like to thank the very helpful staff at the Calar Alto Observatory for their assistance in carrying out our observations. In particular, we would like to thank S. Pedraz, G. Bergond and F. Hoyo for organizing and carrying out service mode observations for us. This research is based on observations collected at the German-Spanish Astronomical Centre, Calar Alto, Spain, operated jointly by the Max-Plank-Institut für Astronomie (MPIA), Heidelberg, and the Spanish National Commission for Astronomy. This research also based in part on observations obtained at Paranal Observatory in ESO program 095.C-0273(A). CG and MM thank DFG for support in projects MU2695/13-1, MU2695/14-1, MU2695/15-1, MU2695/16-1, MU2695/18-1, MU2695/20-1, MU2695/22-1, MU2695/23-1. HA acknowledges support from the Millennium Science Initiative (Chilean Ministry of Economy), through grant 'Nucleus P10-022-F' and from FONDECYT grant 3150643. MS thanks Piezosystem Jena for financial support. SPHERE is an instrument designed and built by a consortium consisting of IPAG (Grenoble, France), MPIA (Heidelberg, Germany), LAM (Marseille, France), LESIA (Paris, France), Laboratoire Lagrange (Nice, France), INAF - Osservatorio di Padova (Italy), Observatoire de Geneve (Switzerland), ETH Zurich (Switzerland), NOVA (Netherlands), ONERA (France) and ASTRON (Netherlands) in collaboration with ESO. SPHERE was funded by ESO, with additional contributions from CNRS (France), MPIA (Germany), INAF (Italy), FINES (Switzerland) and NOVA (Netherlands). SPHERE also received funding from the European Commission Sixth and Seventh Framework Programmes as part of the Optical Infrared Coordination Network for Astronomy (OPTICON) under grant number RII3-Ct-2004-001566 for FP6 (2004-2008), grant number 226604 for FP7 (2009-2012) and grant number 312430 for FP7 (2013-2016). This research has made use of the SIMBAD data base as well as the VizieR catalogue access tool, operated at CDS, Strasbourg, France. This research has made use of NASA's Astrophysics Data System Bibliographic Services. Finally, CG would like to thank Donna Keeley for language editing of the manuscript.

REFERENCES

Abazajian K. N. et al., 2009, ApJS, 182, 543
Adams E. R., Ciardi D. R., Dupree A. K., Gautier T. N., III, Kulesa C., McCarthy D., 2012, AJ, 144, 42
Ahn C. P. et al., 2012, ApJS, 203, 21
Allard F., Homeier D., Freytag B., 2011, in Johns-Krull C., Browning M. K., West A. A., eds, ASP Conf. Ser. Vol. 448, 16th Cambridge Workshop on Cool Stars, Stellar Systems, and the Sun. Astron. Soc. Pac., San Francisco, p. 91
Barclay T. et al., 2013, Nature, 494, 452
Beuzit J.-L. et al., 2008, in McLean I. S. Casali M. M., eds, Proc. SPIE Conf. Ser. Vol. 7014, Ground-based and Airborne Instrumentation for Astronomy II. SPIE, Bellingham, p. 701418
Bonfanti A., Ortolani S., Piotto G., Nascimbeni V., 2015, A&A, 575, A18
Borgniet S. et al., 2014, A&A, 561, A65
Bouwman J., Lawson W. A., Dominik C., Feigelson E. D., Henning Th., Tielens A. G. G. M., Waters L. B. F. M., 2006, ApJ, 653, L57
Chabrier G., 2001, ApJ, 554, 1274
Chauvin G., Beust H., Lagrange A.-M., Eggenberger A., 2011, A&A, 528, A8
Cutri R. M. et al., 2003, 2MASS All Sky Catalog of point sources, NASA/IPAC, available at: http://irsa.ipac.caltech.edu/applications/Gator/
Daemgen S., Hormuth F., Brandner W., Bergfors C., Janson M., Hippler S., Henning T., 2009, A&A, 498, 567
Diolaiti E., Bendinelli O., Bonaccini D., Close L. M., Currie D. G., Parmeggiani G., 2000, in Wizinowich P. L., ed., Proc. SPIE Conf. Ser. Vol. 4007, Adaptive Optical Systems Technology. SPIE, Bellingham, p. 879
Dohlen K. et al., 2008, in McLean I. S. Casali M. M., eds, Proc. SPIE Conf. Ser. Vol. 7014, Ground-based and Airborne Instrumentation for Astronomy II. SPIE, Bellingham, p. 70143L
Dressing C. D., Adams E. R., Dupree A. K., Kulesa C., McCarthy D., 2014, AJ, 148, 78
Eggenberger A., Udry S., Chauvin G., Beuzit J.-L., Lagrange A.-M., Ségransan D., Mayor M., 2007, A&A, 474, 273
Fabrycky D., Tremaine S., 2007, ApJ, 669, 1298
Fressin F. et al., 2011, ApJS, 197, 5
Gilliland R. L. et al., 2013, ApJ, 766, 40
Ginski C., Mugrauer M., Seeliger M., Eisenbeiss T., 2012, MNRAS, 421, 2498
Girardi L., Groenewegen M. A. T., Hatziminaoglou E., da Costa L., 2005, A&A, 436, 895
Hartman J. D. et al., 2011a, ApJ, 726, 52
Hartman J. D. et al., 2011b, ApJ, 742, 59
Hormuth F., Hippler S., Brandner W., Wagner K., Henning T., 2008, in McLean I. S., Casali M. M. eds, Proc. SPIE Conf. Ser. Vol. 7014, Ground-based and Airborne Instrumentation for Astronomy II. SPIE, Bellingham, p. 701448
Howell S. B. et al., 2012, ApJ, 746, 123
Jester S. et al., 2005, AJ, 130, 873
Kimble R. A., MacKenty J. W., O'Connell R. W., Townsend J. A., 2008, in Proc. SPIE Conf. Ser. Vol. 7010, Space Telescopes and Instrumentation 2008: Optical, Infrared, and Millimeter. SPIE, Bellingham, p. 70101E
Kley W., Nelson R., 2007, preprint (arXiv:e-prints)
Kraus A. L., Ireland M. J., Hillenbrand L. A., Martinache F., 2012, ApJ, 745, 19
Laher R. R., Gorjian V., Rebull L. M., Masci F. J., Fowler J. W., Helou G., Kulkarni S. R., Law N. M., 2012, PASP, 124, 737
Latham D. W. et al., 2011, ApJ, 732, L24
Law N. M., Mackay C. D., Baldwin J. E., 2006, A&A, 446, 739
Lee B.-C., Han I., Park M.-G., 2013, A&A, 549, A2
Lee B.-C., Han I., Park M.-G., Mkrtichian D. E., Hatzes A. P., Kim K.-M., 2014, A&A, 566, A67
Lillo-Box J., Barrado D., Bouy H., 2012, A&A, 546, A10
Lillo-Box J., Barrado D., Bouy H., 2014, A&A, 566, A103
Maire A.-L. et al., 2015, A&A, preprint (arXiv:e-prints)
Mason B. D., Wycoff G. L., Hartkopf W. I., Douglass G. G., Worley C. E., 2001, AJ, 122, 3466
Mathieu R. D., Ghez A. M., Jensen E. L. N., Simon M., 2000, in Mannings V., Boss A.P., Russell S. S., eds, Protostars and Planets IV. Univ. Arizona Press, Tucson, AZ, 703
Monet D. G. et al., 2003, AJ, 125, 984
Moutou C. et al., 2011, A&A, 527, A63
Moutou C. et al., 2014, A&A, 563, A22
Mugrauer M., Ginski C., 2015, MNRAS, 450, 3127
Mugrauer M., Neuhäuser R., Mazeh T., 2007, A&A, 469, 755
Mugrauer M., Ginski C., Seeliger M., 2014, MNRAS, 439, 1063

Muirhead P. S. et al., 2012, ApJ, 747, 144
Naoz S., Farr W. M., Lithwick Y., Rasio F. A., Teyssandier J., 2011, Nature, 473, 187
Narita N. et al., 2010, PASJ, 62, 779
Ngo H. et al., 2015, ApJ, 800, 138
Niedzielski A., Nowak G., Adamów M., Wolszczan A., 2009, ApJ, 707, 768
Ofek E. O., 2008, PASP, 120, 1128
Paardekooper S.-J., Thébault P., Mellema G., 2008, MNRAS, 386, 973
Pace G., 2013, A&A, 551, L8
Pál A. et al., 2008, ApJ, 680, 1450
Petrovich C., 2015, ApJ, 799, 27
Quinn S. N. et al., 2014, ApJ, 787, 27
Rafikov R. R., 2013, ApJ, 764, L16
Raghavan D., Henry T. J., Mason B. D., Subasavage J. P., Jao W.-C., Beaulieu T. D., Hambly N. C., 2006, ApJ, 646, 523
Raghavan D. et al., 2010, ApJS, 190, 1
Ramírez I., Fish J. R., Lambert D. L., Allende Prieto C., 2012, ApJ, 756, 46
Rasio F. A., Ford E. B., 1996, Science, 274, 954
Riddle R. L. et al., 2015, ApJ, 799, 4
Roberts L. C., Jr, Tokovinin A., Mason B. D., Riddle R. L., Hartkopf W. I., Law N. M., Baranec C., 2015, AJ, 149, 118
Robertson P. et al., 2012, ApJ, 749, 39
Robertson P., Endl M., Cochran W. D., MacQueen P. J., Boss A. P., 2013, ApJ, 774, 147
Roell T., Neuhäuser R., Seifahrt A., Mugrauer M., 2012, A&A, 542, A92
Sanchis-Ojeda R. et al., 2013, ApJ, 775, 54
Skrutskie M. F. et al., 2006, AJ, 131, 1163
Soubiran C., Bienaymé O., Mishenina T. V., Kovtyukh V. V., 2008, A&A, 480, 91
Strehl K., 1902, Z. Instrum., 22, 213
Takeda G., Rasio F. A., 2005, ApJ, 627, 1001
Takeda Y., Sato B., Murata D., 2008, PASJ, 60, 781
Thebault P., Haghighipour N., 2014, preprint (arXiv:e-prints)
Torres G., Konacki M., Sasselov D. D., Jha S., 2004, ApJ, 614, 979
van Leeuwen F., 2007, A&A, 474, 653
Vigan A., Moutou C., Langlois M., Allard F., Boccaletti A., Carbillet M., Mouillet D., Smith I., 2010, MNRAS, 407, 71
Walkowicz L. M., Basri G. S., 2013, MNRAS, 436, 1883
Wang J., Fischer D. A., Xie J.-W., Ciardi D. R., 2015, ApJ, 813, 130
West R. G. et al., 2016, A&A, 585, A126
Wöllert M., Brandner W., 2015, A&A, 579, A129
Wöllert M., Brandner W., Bergfors C., Henning T., 2015, A&A, 575, A23
York D. G. et al., 2000, AJ, 120, 1579
Zacharias N., Finch C. T., Girard T. M., Henden A., Bartlett J. L., Monet D. G., Zacharias M. I., 2013, AJ, 145, 44

SUPPORTING INFORMATION

Additional Supporting Information may be found in the online version of this article:

multiplicity_addendum.pdf
(http://www.mnras.oxfordjournals.org/lookup/suppl/doi:10.1093/mnras/stw049/-/DC1).

Please note: Oxford University Press is not responsible for the content or functionality of any supporting materials supplied by the authors. Any queries (other than missing material) should be directed to the corresponding author for the article.

This paper has been typeset from a TEX/LATEX file prepared by the author.